thrombocytopenic NOG mice and high-spatiotemporal-resolution confocal laser microscopy to visualize the initial adhesion of individual platelets to laser-exposed vessel walls and the subsequent thrombus formation under flow conditions without apparent endothelial disruption (Takizawa et al., 2010; Nishimura et al., 2012). Using fresh human platelets or imMKCL-derived platelets labeled with carboxyfluorescein diacetate and succinimidyl ester, along with injection of Texas Red dextran to visualize blood cell kinetics, we calculated the numbers of platelets adhering to the endothelium after laser injury in the NOG system (Movie S2). We confirmed that single imMKCL-derived platelets adhere to the vessel without forming aggregates with host platelets. AK4 antibody (antihuman P-selectin) partly reversed the platelet adhesion (i.e., >60% for Cl-2 platelets; Figure 6C), indicating that P-selectin contributed to the initial adhesion of the imMKCL platelets and that endothelial-derived vWF and P-selectin are relevant in our mouse models (Nishimura et al., 2012). We also confirmed the contribution of these platelets to thrombi in vivo. We found that platelets from four different imMKCL clones differentially contributed to the developing thrombi to a degree that was at a minimum better than human endogenous pooled platelets ($n = 40$ vessels from three to five animals individually, $p < 0.0001$; Figures 6D and 6E and Movie S3), suggesting that transfer to in vivo conditions may further improve the functionality of imMKCL platelets, perhaps through rejuvenation via endocytosis of granules. Accordingly, our results suggest that, although imMKCL platelets display a smaller capacity for adhesion and aggregation than fresh donor platelets in vitro and in vivo, the functional capacity observed is at a useful level and could potentially be improved by further optimization of the culture conditions and/or the collection method.

DISCUSSION

For successful clinical application of hiPSC technology to platelet transfusion, it will be necessary to produce very large quantities of platelets. To achieve this goal, we will need to boost production efficiency at two stages: the transition from HSCs or myeloid lineage HPCs to MKs and the transition from MKs to platelets (Fuentes et al., 2010; Lu et al., 2011; Takayama et al., 2010; Lambert et al., 2013; Yamamoto et al., 2013). In the present report, we focused on a strategy of generating self-renewing immortalized MKs (Yamamoto et al., 2013), and we have succeeded in establishing imMKCLs with in vitro long-term expansion capacity from human ESCs or iPSCs with three defined factors (c-MYC, BMI1, and BCL-XL) with a temporally hierarchical overexpression protocol (Figures 2 and S3D–S3G). Sustained expansion of these imMKCLs relied on carefully regulated expression of the inducing genes to balance proliferative and apoptotic signals and optimize consistent proliferation. These self-replicating MKs may be applicable in the clinic as a source for a continuous and virtually inexhaustible supply of platelets.

We also showed that the INK4A/ARF and caspase 3 and 7 pathways are activated at the MK progenitor stage when c-MYC levels are too high. The DD derived from mutant human FKBP12 contributes to instability of the tagged protein, but the effect is attenuated by addition of Shield1 (Banaszynski et al., 2006). By using a DD tag vector system as a tool for investigating the impact of restricted c-MYC levels (Figures 1E–1G and S1G), we confirmed the importance of reducing caspase activity during immortalized self-replication of the MK lineage in the presence of TPO and SCF, which suggests that caspase activity plays a role in the previously observed unstable proliferation of MKs in vitro (Figures 7A–7C). This "constrained protein expression" system could also be useful for studying genes that must be strictly regulated. These findings also suggest the existence of a regulatory pathway distinct from the INK4A/ARF and p53 pathways that exerts a protective effect against oncogenic stress in the MK lineage (Figure 2F).

Exogenous overexpression of *BCL-XL* contributed to long-term self-replication by attenuating caspase 3 and 7 activation, even in the presence of higher c-MYC levels (Figure 7C), and endogenous BCL-XL may be required for the survival of imMKCLs yielding platelets (Figures S5A and S5B). Consistent with that idea, results obtained with BCL-XL-deficient mice indicate that this protein is required for MK survival and platelet release (Josefsson et al., 2011). By contrast, sustained BCL-XL overexpression reportedly has a negative effect on the development of demarcation membranes in MKs and on platelet production (Kaluzhny et al., 2002). However, c-MYC-dependent MK proliferation was also TPO-dependent and required BMI1 to be present prior to BCL-XL (Figures 1C, 2C, 2D, and S3D–S3G). Interestingly, we recently showed that the combination of c-MYC and BCL-XL overexpression in $CD34^+CD43^+$-containing HPCs leads to stable erythroblast self-replication induced by erythropoietin (Hirose et al., 2013) but not MK lineage growth (Figure 1C). Thus, distinct combinations of c-MYC and BCL-XL and c-MYC and BMI1 appear to provide context-dependent expansion capacity for erythroblast or MK lineages, respectively (Hirata et al., 2013; Yamamoto et al., 2013). It has also been reported that BMI1 directly binds to RUNX1 and core binding transcriptional factor β and acts as a regulator during megakaryopoiesis (Yu et al., 2012), suggesting that BMI1 may have an alternative function in imMKCL development. The MK proliferation program may be disrupted when the effects of BCL-XL dominate before the MK proliferation program is fully established.

For clinical application, the quality of expandable imMKCLs must be strictly validated, and they must be cryopreserved as master cell banks (MCBs) matched to the required HLA and HPA type. After thawing, MCB-derived working cells would be expected to grow within an appropriate and sufficient term and

(C) Numbers of $CD41a^+CD42b^+$ platelets generated from imMKCL Cl-2 (KhES3) and Cl-7 (DN-SeV2) in a 1 ml culture volume. White bars, genes on; black bars, genes off. Results are expressed as means ± SE from three independent experiments.

(D) Histograms show CD42b, CD49b, CD61, PAR1, GPVI, and CD29 expression on platelets (fresh and pooled) derived from normal donors (two different donors) and imMKCL Cl-2 and Cl-7. Donor-derived pooled platelets were pooled at 37°C for 5 days. Fresh human platelets were from donors 1 (purple) or 2 (green). Pooled platelets were from donor 1. imMKCL platelets were from Cl-2 (yellow) and Cl-7 (red). Black lines in all panels indicate IgG control. x axes, MFI (log scale); axes, counts.

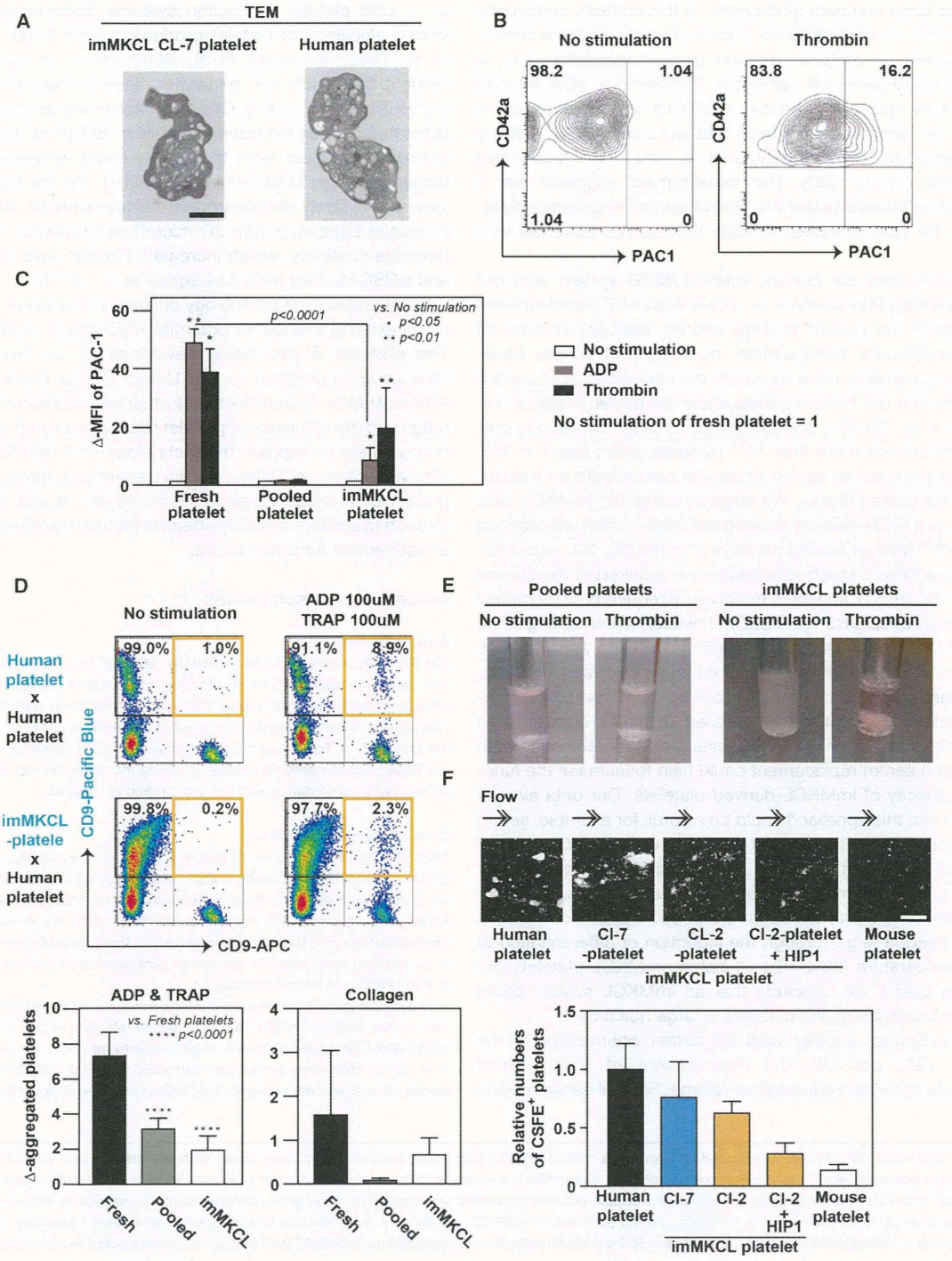

Figure 5. Characterization of imMKCL-Derived Platelets In Vitro

(A) Transmission electron micrographs of an imMKCL Cl-7-derived platelet 5 days after genes off (left) and two fresh donor platelets (right). The imMKCL platelet shows fewer a-granules and dense granules than fresh platelets. The scale bar represents 1 μm.

(B) Representative contour plots for imMKCL platelets showing CD42a (GPIX) and PAC1 bound in the absence or presence of thrombin (1 u/ml).

(C) PAC1 binding to human fresh platelets, human pooled platelets, or imMKCL platelets was quantified by flow cytometry. Data depict means (± SEM) from three independent experiments. y axis indicates ΔMFI calculated as agonist (+) minus no agonist (−). The MFI of agonist (−) was 1.0 in individual samples. ADP (200 μM) or thrombin (1 u/ml) was the agonist.

(legend continued on next pa

Please cite this article in press as: Nakamura et al., Expandable Megakaryocyte Cell Lines Enable Clinically Applicable Generation of Platelets from Human Induced Pluripotent Stem Cells, Cell Stem Cell (2014), http://dx.doi.org/10.1016/j.stem.2014.01.011

generate large numbers of platelets. In this context, continuous culture after cryopreservation (Figure 2E) may enable a continuous supply of platelets through gene manipulation (i.e., a drug-induced genes-off condition). Furthermore, after we had established stably expandable imMKCLs in the presence of serum, we identified two clones that were capable of growing well in liquid culture after adaptation to serum- and feeder-free conditions (Figure S6D). This development suggests that it may well be feasible to use this type of system to generate platelets on the type of industrial scale that can be achieved with tanks.

We compared our current imMKCL/MCB system with our earlier strategy (Takayama et al., 2010). Figure S7 depicts the advantages of the current strategy and its feasibility in terms of three parameters: manipulation, duration, and culture scale. For each parameter in the figure, the top panels show our current protocol, and the bottom panels show the earlier protocol (Takayama et al., 2010). It is important to consider the need to prepare and provide more than 10^{11} platelets, given that 3×10^{11} platelets are required for 1 u of platelet concentrate for transfusion in the United States. We suggest using 10^8 imMKCL cells per vial as a MCB-derived working cell stock, which will produce 2.5×10^{10} MKs in around 14 days (Figures 2C, 2D, and S3D–S3G). In addition, much less medium is required in the current system (Figure S7), and there might be no requirement for mouse feeder cells or serum (Figure S6D). However, when looking at the similarity between human endogenous platelets and imMKCL platelets, there were several discrepancies between the functional parameters in vitro and in vivo (Figures 6C and 6D). In general, platelet concentrate is supplied in highly concentrated serum for transfusion. This suggests that supplementing with serum or a serum replacement could help to increase the functional capacity of imMKCL-derived platelets. Our data already suggest that this approach could be helpful; for example, serum supplementation improved clot retraction with imMKCL-derived platelets (Figure 5E). This is in contrast to endogenous pooled platelets, which did not form clots at all, even with serum supplementation. Therefore, although further optimization of this final step is needed (e.g., through the induction of differentiation at room temperature (20°C –24°C) before imMKCL platelets are clinically useful, we conclude that an imMKCL system could potentially provide useful platelets in large quantities.

As mentioned, another area for further optimization is the platelet yield per MK, the improvement of which would contribute to further reducing the volume. Several earlier reports on in vitro platelet production systems documented similarly limited efficiency of platelet production from single MKs (Ono et al., 2012; Takayama et al., 2008, 2010). In contrast, it is thought that each MK generates several thousand platelets in vivo (Patel et al., 2005). One approach could be to use a bioreactor that mimics the conditions within BM (Patel et al., 2005), where shear stress from blood flow might accelerate platelet biogenesis from MKs (Junt et al., 2007). On the basis of that idea, we recently demonstrated the feasibility of an artificially produced bioreactor with 2D microfluid circulation and biodegradable scaffolds, which increased platelet yield from hESC- and hiPSC-derived MKs (Nakagawa et al., 2013).

In conclusion, the technology outlined in this study sheds light on an exciting avenue for potential iPSC-based platelet supply. This protocol is also being developed for an Investigational New Drug Application to the United States Food and Drug Administration. To achieve that, further optimization of MK maturation and the efficiency of platelet release in a liquid culture system will help to improve the technology as it develops toward clinical application. Ultimately, we believe that, through the integration of a broad range of technologies, it will be feasible through to achieve clinically effective platelet transfusion without a requirement for donor blood.

EXPERIMENTAL PROCEDURES

Ethical Review

KhES-3 hESC clone (Institute for Frontier Medical Science, Kyoto University) was used with approval from the Ministry of Education, Culture, Sports, Science and Technology of Japan. Collection of PB from healthy volunteers was approved by the ethics committee of the Institute of Medical Science at the University of Tokyo and the Kyoto University Committee for Human Sample-Based Experiments. All studies involving the use of human samples were conducted in accordance with the Declaration of Helsinki.

Cells, Reagents, and Mice

KhES-3 hESCs from H. Suemori (Suemori et al., 2006) and human iPSC clones (585A1, 585B1, 606A1, 648B1, 692D2, and DNSeV-2) were used (Okita et al., 2013). Six-week-old NOG mice were purchased from the Central Institute for Experimental Animals. The mice were irradiated at 2.4 Gy in order to induce thrombocytopenia 9 days before transfusion. Then, selected mice (platelets = 5–20 $\times 10^4/\mu l$) were used for studies of posttransfusion platelet kinetics and in vivo imaging of thrombogeneity.

The following vectors were used: pMXs retroviral vector, pGCDNsam retroviral vector, modified pMXs Tet off-inducible retroviral vector (Ohmine et al., 2001), and CSII-based all-in-one inducible lentiviral vector (Ai-LV) (Takayama et al., 2010). Retrovirus production with a 293 Gag, Pol, VSV-G (vesicular stomatitis virus G) system and lentiviral production were as described previously

(D) Flow cytometric detection of aggregated platelets as a double-positive population among human fresh donor platelets stained with CD9-APC or among human fresh donor platelets (top panel in the dot plot) or with imMKCLs platelets (bottom panel in the dot plot) stained with CD9 Pacific Blue after agonist stimulation. In the absence of agonist stimulation, the double-positive population was small. The lower graph contains summarized results showing the percent double-positive platelets (human fresh platelets, pooled platelets, or imMKCL platelets). y axis indicates D-aggregated percentage calculated as agonist (+) minus agonist (–).Results are expressed as means ± SE from seven independent experiments for ADP&TRAP (left) or four independent experiments for collagen (right).

(E) Pictures of clot retraction. Human endogenous pooled or imMKCL (Cl-7) platelets were suspended in 20% platelet-depleted human plasma containing Iscove's modified Dulbecco's medium (1.6×10^8 platelets/ml). Even when supplemented with human plasma, pooled platelets stored without serum showed no clot retraction, whereas imMKCL platelets did.

(F) Ex vivo flow chamber system within which human vWF (10 μg/ml) was immobilized, and the shear rate was 1,600 s^{-1}. Human and mouse PB platelets and imMKCL Cl-2 and Cl-7 platelets were stained with carboxyfluorescein diacetate, succinimidyl ester (CSFE) and analyzed. Top: representative immunofluorescence micrograph of the chamber. Bottom: relative number of $CSFE^+$ platelets adhering to human vWF. HIP-1, human CD42b antibody. The scale bar represents 100 μm. Results are expressed as means ± SE of a total of 20 trials from three independent experiments. The mean value of human platelets is assigned as 1.0.

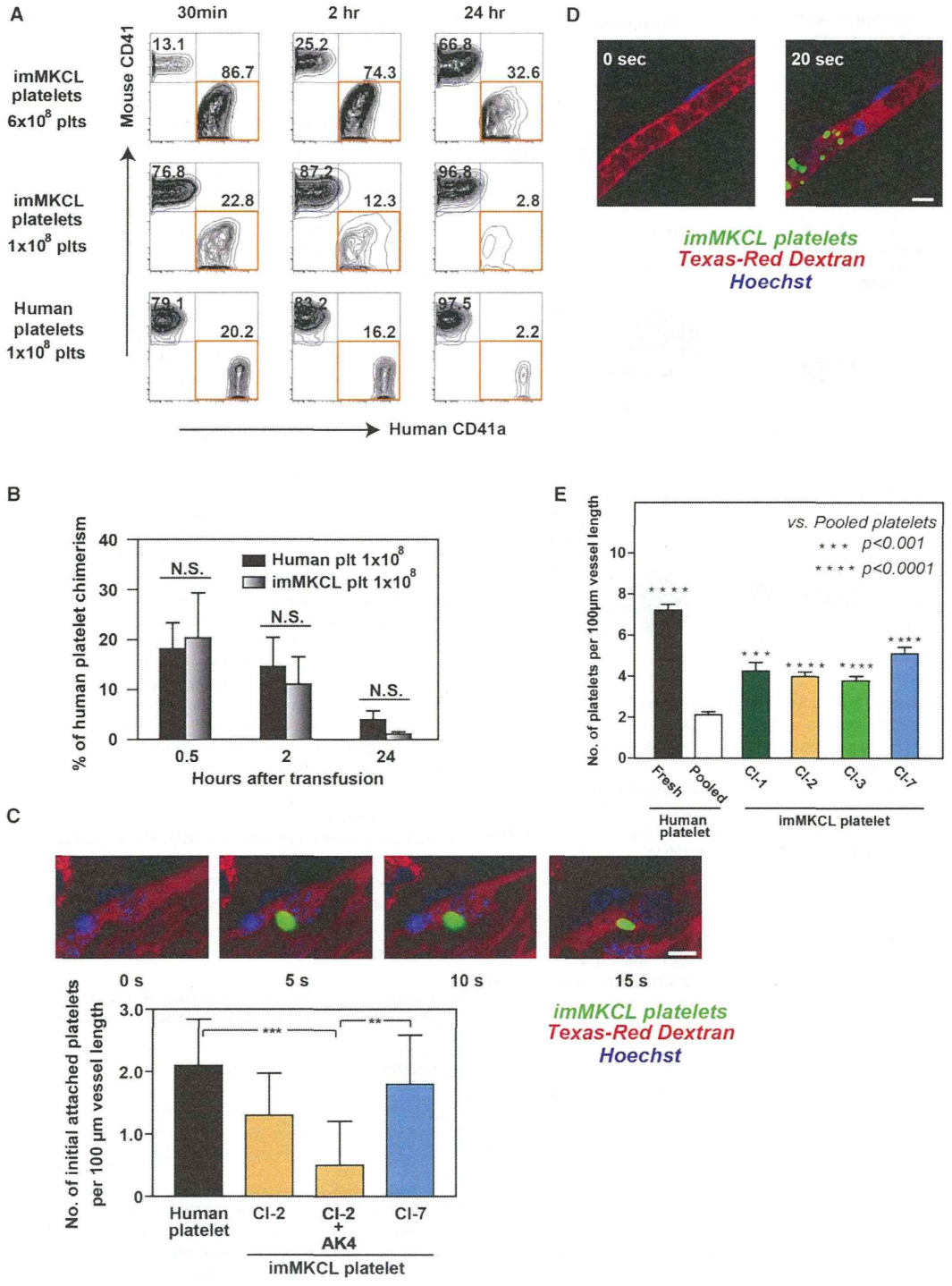

Figure 6. imMKCL-Derived Platelets Show Circulation Potential and Intact In Vivo Functionality in a Thrombocytopenic Mouse Model

(A) Platelet transfusion model in which NOG mice were irradiated (2.4 Gy) in order to induce thrombocytopenia. Nine days later, imMKCL-derived platelets (6×10^8 or 1×10^8) and human PB-derived platelets (1×10^8) were injected via the tail vein. Shown are representative contour plots of samples from a transfused mouse. Detected are mouse $CD41^+$ and human $CD41a^+$ cells 30 min, 2 hr, and 24 hr after transfusion.

(B) Platelet chimerism was quantified by flow cytometry. Circulation of injected platelets was evaluated after 30 min, 2 hr, and 24 hr. N = 4 individual groups from two independent experiments.

(legend continued on next page)

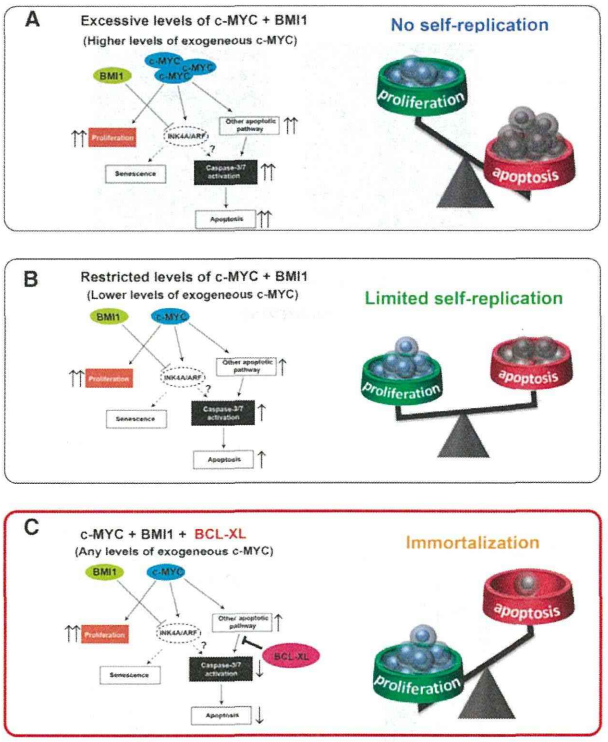

Figure 7. Models of MKCL Self-Replication Systems

(A) Excessive c-MYC induces strong activation of caspase 3 and 7 and apoptotic pathways, despite the suppression of INK4A/ARF by ectopic BMI1, leading to no self-replication.

(B) Appropriate activation of c-MYC induces a relatively low level of caspase 3 and 7 activation, leading to limited self-replication.

(C) Added BCL-XL acts in concert with BMI1 to suppress c-MYC-related apoptotic pathways, leading to MKCL immortalization.

(Eto et al., 2007; Takayama et al., 2010). We amplified the DD-encoding sequence from pPTunerC vector and Shield1 (Clontech and Takara Biotechnology) to generate the *cMYC-DD* construct. Shield1 was used to block DD-domain-mediated protein degradation. The use of viral vectors was approved by committees at the University of Tokyo or Kyoto University.

Cell Culture

On day 14 of culture, during hematopoietic differentiation from hESCs and hiPSCs (Takayama et al., 2008), HPCs were collected and transferred onto irradiated C3H10T1/2 cells in the presence of 50 ng/ml human SCF (R&D Systems) and 50 ng/ml human TPO (R&D) (Takayama et al., 2010). Gene expression was controlled by the presence or absence of 2 μM β-estradiol or 1 μg/ml doxycycline (Clontech) for modified pMXs inducible vector or the presence of 1 μg/ml doxycycline for Ai-LV, respectively. MK differentiation from CB $CD34^+$ cell was accomplished as described previously (Proulx et al., 2004).

In Vitro Analysis of imMKCLs, imMKCL Platelets, and Human Platelets

qRT-PCR, cell-surface markers of imMKCLs and platelets, electron microscopy, and PAC-1 binding were examined as described previously (Takayama et al., 2010). Flow-cytometry-based platelet aggregation assays were performed as described previously (De Cuyper et al., 2013). Clot retraction assays were carried out as described previously (Takizawa et al., 2010). An ex vivo flow chamber precoated with human vWF (10 μg/ml, provided by K. Soejima, Kaketsuken) was utilized to observe shear (1,600 s^{-1})-dependent thrombus formation under an inverted microscope equipped with fluorescence (Nikon A1R) and microfluid systems (Ibidi Products). Platelets were stained with CFSE dye (5 μM, Invitrogen) and used in the presence of CD42b (HIP1; Abcam; 10 μg/ml) or isotype-matched antibodies (BioLegend). Human pooled platelets were prepared by 5-day culture at 37°C under serum-free conditions.

In Vivo Analysis in Mice

Nine days later, irradiation in NOG mice, fresh or pooled human platelets from a donor, or imMKCL-derived platelets were intravenously administered (100 μl). Then, blood samples (50–100 μl) were collected from the retro-orbital plexus in the mice 30 min, 2 hr, and 24 hr after transfusion. The samples were labeled with human CD41a-APC and mouse CD41-PE antibodies (EMFRET Analytics), after which chimerism was analyzed. Similar NOG mice with thrombocytopenia were also used for in vivo imaging studies. To visually analyze thrombus formation in the microcirculation of the mesentery in living animals, we used in vivo laser- and reactive-oxygen-species-induced injury with a visualization technique developed through modification of conventional methods (Nishimura et al., 2012; Takizawa et al., 2010). Some experiments were performed with AK4 (human P-selectin antibody; Abcam; 20 μg/ml). Additional details of the methods and other information for imaging are presented in the Supplemental Information.

Statistical Analysis

All data are presented as means ± SEM. The statistical significance of the observed differences was determined with one-way ANOVA followed by Tukey's multiple comparison test and two-tailed Student's t tests for pairwise comparisons. Values of $p < 0.05$ were considered significant.

ACCESSION NUMBERS

Raw and normalized microarray data have been deposited in the NCBI Gene Expression Omnibus database under accession number GSE54168.

SUPPLEMENTAL INFORMATION

Supplemental Information contains Supplemental Experimental Procedures, seven figures, and three movies and can be found with this article online at http://dx.doi.org/10.1016/j.stem.2014.01.011.

(C) Time-lapse confocal microscopy showing potential in vivo platelet function. Mice were transfused with 1×10^8 platelets derived from different groups. Top: representative sequential images showing initial adhesion by imMKCL-derived platelets onto injured vessel walls. CSFE-labeled imMKCL platelets (Cl-2 and Cl-7; green) along with dextran (Texas Red) are shown. Bottom: the number of initially attached platelets per 100 μm vessel length were counted. Actual results are shown in Movie S2. The results are averaged data from 40 vessels from three to five animals in each group. N.S., not significant; ***$p < 0.001$, ****$p < 0.0001$. AK4; human P-selectin antibody. The scale bar represents 10 μm.

(D) Representative sequential images showing thrombus formation by imMKCL-derived platelets within a small capillary and artery. CSFE-labeled imMKCL platelets (green) along with dextran (Texas Red) are shown. Hematoporphyrin was administrated in order to induce thrombus formation prior to laser-induced injury. Platelets adhered to the site of laser injury, finally contributing to the complete occlusion of vessels. Original videos are available as Movie S3. The scale bars represent 10 μm.

(E) Fresh donor platelets, pooled donor platelets, and imMKCL-derived platelets incorporated into thrombi were quantified. Pooled platelets were stored for 5 days at 37°C. Platelets from imMKCL Cl-1, Cl-2, Cl-3, and Cl-7 were used. The results summarize four independent experiments (n = 40 vessels from three to five animals for each group). N.S., not significant; ***$p < 0.001$, ****$p < 0.0001$.

ACKNOWLEDGMENTS

The authors thank H. Suemori, T. Kitamura, M. Onodera, H. Mano, M. Nakanishi, R. Mulligan, H. Kashiwagi, K. Soejima, and Y. Kurose. Electron microscopy was supported by Integrated Imaging Research Support (nonprofit organization). This work was supported by grants-in-aid from MEXT (K.E.) and the Project of Realization of Regenerative Medicine and Highway Program from MEXT/JST (K.E.), A-STEP, and CREST from JST (K.E.) and a Health Labor Sciences Research Grant from the Ministry of Health Labor and Welfare (K.E.). This research was also supported in part by the first Program from JSPS (S.Y.). Visiting fellows S.H. (Kaken Pharmaceutical), T.K. (Nissan Chemical), and K.H. (Toray Industries) were supported by each company. S.Y. is a member without salary of scientific advisory board (SAB) of iPierian, iPS Academia Japan, Megakaryon, and HEALIOS K. K. Japan. H.N. and K.E. are members without salary of SAB of Megakaryon. H.N. is an outside board member of ReproCELL. S.N., N.T., H.N., and K.E. submitted the patent related with this manuscript.

Received: January 31, 2013
Revised: October 2, 2013
Accepted: January 12, 2014
Published: February 13, 2014

REFERENCES

Banaszynski, L.A., Chen, L.C., Maynard-Smith, L.A., Ooi, A.G., and Wandless, T.J. (2006). A rapid, reversible, and tunable method to regulate protein function in living cells using synthetic small molecules. Cell *126*, 995–1004.

Bergmeier, W., Burger, P.C., Piffath, C.L., Hoffmeister, K.M., Hartwig, J.H., Nieswandt, B., and Wagner, D.D. (2003). Metalloproteinase inhibitors improve the recovery and hemostatic function of in vitro-aged or -injured mouse platelets. Blood *102*, 4229–4235.

Chen, C., Fuhrken, P.G., Huang, L.T., Apostolidis, P., Wang, M., Paredes, C.J., Miller, W.M., and Papoutsakis, E.T. (2007). A systems-biology analysis of isogenic megakaryocytic and granulocytic cultures identifies new molecular components of megakaryocytic apoptosis. BMC Genomics *8*, 384.

De Cuyper, I.M., Meinders, M., van de Vijver, E., de Korte, D., Porcelijn, L., de Haas, M., Eble, J.A., Seeger, K., Rutella, S., Pagliara, D., et al. (2013). A novel flow cytometry-based platelet aggregation assay. Blood *121*, e70–e80.

Eto, K., Nishikii, H., Ogaeri, T., Suetsugu, S., Kamiya, A., Kobayashi, T., Yamazaki, D., Oda, A., Takenawa, T., and Nakauchi, H. (2007). The WAVE2/Abi1 complex differentially regulates megakaryocyte development and spreading: implications for platelet biogenesis and spreading machinery. Blood *110*, 3637–3647.

Fuentes, R., Wang, Y., Hirsch, J., Wang, C., Rauova, L., Worthen, G.S., Kowalska, M.A., and Poncz, M. (2010). Infusion of mature megakaryocytes into mice yields functional platelets. J. Clin. Invest. *120*, 3917–3922.

Gardiner, E.E., Al-Tamimi, M., Andrews, R.K., and Berndt, M.C. (2012). Platelet receptor shedding. Methods Mol. Biol. *788*, 321–339.

Hirata, S., Takayama, N., Jono-Ohnishi, R., Endo, H., Nakamura, S., Dohda, T., Nishi, M., Hamazaki, Y., Ishii, E.I., Kaneko, S., et al. (2013). Congenital amegakaryocytic thrombocytopenia iPS cells exhibit defective MPL-mediated signaling. J. Clin. Invest. *123*, 3802–3814.

Hirose, S., Takayama, N., Nakamura, S., Nagasawa, K., Ochi, K., Hirata, S., Yamazaki, S., Yamaguchi, T., Otsu, M., Sano, S., et al. (2013). Immortalization of erythroblasts by c-MYC and BCL-XL enables large-scale erythrocyte production from human pluripotent stem cells. Stem Cell Reports *1*, 499–508.

Hotti, A., Järvinen, K., Siivola, P., and Hölttä, E. (2000). Caspases and mitochondria in c-Myc-induced apoptosis: identification of ATM as a new target of caspases. Oncogene *19*, 2354–2362.

Isakari, Y., Sogo, S., Ishida, T., Kawakami, T., Ono, T., Taki, T., and Kiwada, H. (2009). Gene expression analysis during platelet-like particle production in phorbol myristate acetate-treated MEG-01 cells. Biol. Pharm. Bull. *32*, 354–358.

Josefsson, E.C., James, C., Henley, K.J., Debrincat, M.A., Rogers, K.L., Dowling, M.R., White, M.J., Kruse, E.A., Lane, R.M., Ellis, S., et al. (2011). Megakaryocytes possess a functional intrinsic apoptosis pathway that must be restrained to survive and produce platelets. J. Exp. Med. *208*, 2017–2031.

Juin, P., Hunt, A., Littlewood, T., Griffiths, B., Swigart, L.B., Korsmeyer, S., and Evan, G. (2002). c-Myc functionally cooperates with Bax to induce apoptosis. Mol. Cell. Biol. *22*, 6158–6169.

Junt, T., Schulze, H., Chen, Z., Massberg, S., Goerge, T., Krueger, A., Wagner, D.D., Graf, T., Italiano, J.E., Jr., Shivdasani, R.A., and von Andrian, U.H. (2007). Dynamic visualization of thrombopoiesis within bone marrow. Science *317*, 1767–1770.

Kaluzhny, Y., Yu, G., Sun, S., Toselli, P.A., Nieswandt, B., Jackson, C.W., and Ravid, K. (2002). BclxL overexpression in megakaryocytes leads to impaired platelet fragmentation. Blood *100*, 1670–1678.

Kumar, S., and Cakouros, D. (2004). Transcriptional control of the core cell-death machinery. Trends Biochem. Sci. *29*, 193–199.

Lambert, M.P., Sullivan, S.K., Fuentes, R., French, D.L., and Poncz, M. (2013). Challenges and promises for the development of donor-independent platelet transfusions. Blood *121*, 3319–3324.

Leytin, V., Allen, D.J., Gwozdz, A., Garvey, B., and Freedman, J. (2004). Role of platelet surface glycoprotein Ibalpha and P-selectin in the clearance of transfused platelet concentrates. Transfusion *44*, 1487–1495.

Lu, S.J., Li, F., Yin, H., Feng, Q., Kimbrel, E.A., Hahm, E., Thon, J.N., Wang, W., Italiano, J.E., Cho, J., and Lanza, R. (2011). Platelets generated from human embryonic stem cells are functional in vitro and in the microcirculation of living mice. Cell Res. *21*, 530–545.

Nakagawa, Y., Nakamura, S., Nakajima, M., Endo, H., Dohda, T., Takayama, N., Nakauchi, H., Arai, F., Fukuda, T., and Eto, K. (2013). Two differential flows in a bioreactor promoted platelet generation from human pluripotent stem cell-derived megakaryocytes. Exp. Hematol. *41*, 742–748.

Nishikii, H., Eto, K., Tamura, N., Hattori, K., Heissig, B., Kanaji, T., Sawaguchi, A., Goto, S., Ware, J., and Nakauchi, H. (2008). Metalloproteinase regulation improves in vitro generation of efficacious platelets from mouse embryonic stem cells. J. Exp. Med. *205*, 1917–1927.

Nishimura, S., Manabe, I., Nagasaki, M., Kakuta, S., Iwakura, Y., Takayama, N., Ooehara, J., Otsu, M., Kamiya, A., Petrich, B.G., et al. (2012). In vivo imaging visualizes discoid platelet aggregations without endothelium disruption and implicates contribution of inflammatory cytokine and integrin signaling. Blood *119*, e45–e56.

Oguro, H., Iwama, A., Morita, Y., Kamijo, T., van Lohuizen, M., and Nakauchi, H. (2006). Differential impact of Ink4a and Arf on hematopoietic stem cells and their bone marrow microenvironment in Bmi1-deficient mice. J. Exp. Med. *203*, 2247–2253.

Ohmine, K., Ota, J., Ueda, M., Ueno, S., Yoshida, K., Yamashita, Y., Kirito, K., Imagawa, S., Nakamura, Y., Saito, K., et al. (2001). Characterization of stage progression in chronic myeloid leukemia by DNA microarray with purified hematopoietic stem cells. Oncogene *20*, 8249–8257.

Okita, K., Yamakawa, T., Matsumura, Y., Sato, Y., Amano, N., Watanabe, A., Goshima, N., and Yamanaka, S. (2013). An efficient nonviral method to generate integration-free human-induced pluripotent stem cells from cord blood and peripheral blood cells. Stem Cells *31*, 458–466.

Ono, Y., Wang, Y., Suzuki, H., Okamoto, S., Ikeda, Y., Murata, M., Poncz, M., and Matsubara, Y. (2012). Induction of functional platelets from mouse and human fibroblasts by p45NF-E2/Maf. Blood *120*, 3812–3821.

Patel, S.R., Hartwig, J.H., and Italiano, J.E., Jr. (2005). The biogenesis of platelets from megakaryocyte proplatelets. J. Clin. Invest. *115*, 3348–3354.

Proulx, C., Dupuis, N., St-Amour, I., Boyer, L., and Lemieux, R. (2004). Increased megakaryopoiesis in cultures of CD34-enriched cord blood cells maintained at 39 degrees C. Biotechnol. Bioeng. *88*, 675–680.

Sato, T., Fuse, A., Eguchi, M., Hayashi, Y., Ryo, R., Adachi, M., Kishimoto, Y., Teramura, M., Mizoguchi, H., Shima, Y., et al. (1989). Establishment of a human leukaemic cell line (CMK) with megakaryocytic characteristics from a Down's syndrome patient with acute megakaryoblastic leukaemia. Br. J. Haematol. *72*, 184–190.

Schiffer, C.A. (2001). Diagnosis and management of refractoriness to platelet transfusion. Blood Rev. *15*, 175–180.

Suemori, H., Yasuchika, K., Hasegawa, K., Fujioka, T., Tsuneyoshi, N., and Nakatsuji, N. (2006). Efficient establishment of human embryonic stem cell lines and long-term maintenance with stable karyotype by enzymatic bulk passage. Biochem. Biophys. Res. Commun. *345*, 926–932.

Takahashi, K., Tanabe, K., Ohnuki, M., Narita, M., Ichisaka, T., Tomoda, K., and Yamanaka, S. (2007). Induction of pluripotent stem cells from adult human fibroblasts by defined factors. Cell *131*, 861–872.

Takayama, N., Nishikii, H., Usui, J., Tsukui, H., Sawaguchi, A., Hiroyama, T., Eto, K., and Nakauchi, H. (2008). Generation of functional platelets from human embryonic stem cells in vitro via ES-sacs, VEGF-promoted structures that concentrate hematopoietic progenitors. Blood *111*, 5298–5306.

Takayama, N., Nishimura, S., Nakamura, S., Shimizu, T., Ohnishi, R., Endo, H., Yamaguchi, T., Otsu, M., Nishimura, K., Nakanishi, M., et al. (2010). Transient activation of c-MYC expression is critical for efficient platelet generation from human induced pluripotent stem cells. J. Exp. Med. *207*, 2817–2830.

Takizawa, H., Nishimura, S., Takayama, N., Oda, A., Nishikii, H., Morita, Y., Kakinuma, S., Yamazaki, S., Okamura, S., Tamura, N., et al. (2010). Lnk regulates integrin alphaIIbbeta3 outside-in signaling in mouse platelets, leading to stabilization of thrombus development in vivo. J. Clin. Invest. *120*, 179–190.

Terui, Y., Furukawa, Y., Kikuchi, J., Iwase, S., Hatake, K., and Miura, Y. (1998). Bcl-x is a regulatory factor of apoptosis and differentiation in megakaryocytic lineage cells. Exp. Hematol. *26*, 236–244.

Ware, J., Russell, S., and Ruggeri, Z.M. (2000). Generation and rescue of a murine model of platelet dysfunction: the Bernard-Soulier syndrome. Proc. Natl. Acad. Sci. USA *97*, 2803–2808.

Wong, C.H., Jenne, C.N., Petri, B., Chrobok, N.L., and Kubes, P. (2013). Nucleation of platelets with blood-borne pathogens on Kupffer cells precedes other innate immunity and contributes to bacterial clearance. Nat. Immunol. *14*, 785–792.

Yamamoto, R., Morita, Y., Ooehara, J., Hamanaka, S., Onodera, M., Rudolph, K.L., Ema, H., and Nakauchi, H. (2013). Clonal analysis unveils self-renewing lineage-restricted progenitors generated directly from hematopoietic stem cells. Cell *154*, 1112–1126.

Yu, M., Mazor, T., Huang, H., Huang, H.T., Kathrein, K.L., Woo, A.J., Chouinard, C.R., Labadorf, A., Akie, T.E., Moran, T.B., et al. (2012). Direct recruitment of polycomb repressive complex 1 to chromatin by core binding transcription factors. Mol. Cell *45*, 330–343.

EUROPEAN JOURNAL OF Haematology

European Journal of Haematology 92 (276–282)

ORIGINAL ARTICLE

TUBB1 mutation disrupting microtubule assembly impairs proplatelet formation and results in congenital macrothrombocytopenia

Shinji Kunishima[1], Satoshi Nishimura[2,3,4], Hidenori Suzuki[5], Masue Imaizumi[6], Hidehiko Saito[7]

[1]Department of Advanced Diagnosis, Clinical Research Center, National Hospital Organization Nagoya Medical Center, Nagoya; [2]Department of Cardiovascular Medicine, The University of Tokyo, Tokyo; [3]Translational Systems Biology and Medicine Initiative, The University of Tokyo, Tokyo; [4]Reserach Division of Cell and Molecular Medicine, Center for Molecular Medicine, Jichi Medical University, Tochigi; [5]Department of Morphological and Biomolecular Research, Graduate School of Medicine, Nippon Medical School, Tokyo; [6]Department of Hematology and Oncology, Miyagi Children's Hospital, Miyagi; [7]Honorary Director, National Hospital Organization Nagoya Medical Center, Nagoya, Japan

Abstract

This report describes a family with *TUBB1*-associated macrothrombocytopenia diagnosed based on abnormal platelet β1-tubulin distribution. A circumferential marginal microtubule band was undetectable, whereas microtubules were frayed and disorganized in every platelet from the affected individuals. Patients were heterozygous for novel *TUBB1* p.F260S that locates at the α- and β-tubulin intradimer interface. Mutant β1-tubulin was not incorporated into microtubules with endogenous α-tubulin, and α-tubulin expression was decreased in transfected Chinese hamster ovary cells. Transduction of mutant β1-tubulin into mouse fetal liver-derived megakaryocytes demonstrated no incorporation of mutant β1-tubulin into microtubules with endogenous α-tubulin and diminished proplatelet formation, leading to the production of fewer, but larger, proplatelet tips. Furthermore, mutant β1-tubulin was not associated with endogenous α-tubulin in the proplatelets. Deficient functional microtubules might lead to defective proplatelet formation and abnormal protrusion-like platelet release, resulting in congenital macrothrombocytopenia.

Key words β1-tubulin; macrothrombocytopenia; microtubules; proplatelet formation; *TUBB1*

Correspondence Shinji Kunishima, PhD, Department of Advanced Diagnosis, Clinical Research Center, National Hospital Organization Nagoya Medical Center, 4-1-1 Sannomaru, Naka-ku, Nagoya 460-0001, Japan. Tel: +81 52 951 1111; Fax: +81 52 951 0664; e-mail: kunishis@nnh.hosp.go.jp

Accepted for publication 12 December 2013

doi:10.1111/ejh.12252

Congenital macrothrombocytopenia is a genetically heterogeneous group of rare platelet disorders, among which *MYH9* disorders/*MYH9*-related disease and Bernard-Soulier syndrome are the most frequent (1–3). Less frequent forms involve defects in signaling pathways and/or components of the cytoskeleton that regulate proplatelet formation and morphology (4, 5). Proplatelets are cytoplasmic extensions of megakaryocytes that are elongated by microtubule-based forces (6). The microtubules are assembled from α- and β-tubulin heterodimers and represent a key component of proplatelet formation and platelet release (7). Expression of the β-tubulin isoform, β1-tubulin, is restricted in megakaryocytes and platelets (8). *Tubb1*-knockout mice show thrombocytopenia and spherical platelets (9). We previously reported the first *TUBB1* mutation affecting microtubule assembly in the context of congenital macrothrombocytopenia (10). Subsequent continuous studies on the differential diagnosis of congenital macrothrombocytopenia detected abnormal β1-tubulin distribution in platelets and revealed a second *TUBB1* mutation that impairs megakaryocyte microtubule organization, proplatelet formation, and platelet morphology.

Materials and methods

Patients

Thrombocytopenia was incidentally identified in 12-year-old dizygotic twin boys (Table 1). Peripheral blood smears

Table 1 Characteristics of platelets from a family with *TUBB1* p.F260S mutation

Individual	Sex	Age (years)	*TUBB1* mutation	Platelet count ($\times 10^9$/L)	Platelet size (μm)[1]	Mean platelet volume[2]	Bleeding tendency	Initial diagnosis
Mother	F	37	p.F260S	104	ND	ND	–	Immune thrombocytopenia
Patient 1	M	12	p.F260S	120	3.0 ± 0.9	ND	–	Unknown thrombocytopenia
Patient 2	M	12	p.F260S	97	3.4 ± 0.9	ND	–	Unknown thrombocytopenia
Sister	F	9	p.F260S	125	3.5 ± 0.6	13.8	–	Unknown thrombocytopenia
Mean ± SD				111.5 ± 13.2	3.3 ± 0.3			

[1]Determined by microscopic observation of 200 platelets on a stained peripheral blood smear. Controls, 2.5 ± 0.3 μm (n = 31).
[2]Normal range, 9.4–12.5.

showed large platelets (Fig. 1A). Neither twin had a bleeding tendency. *MYH9* disorders, heterozygous and homozygous Bernard-Soulier syndrome, and glycoprotein (GP) IIb/IIIa-associated macrothrombocytopenia were excluded by immunofluorescence analysis for granulocyte myosin IIA and by flow cytometry for platelet GPIb/IX and GPIIb/IIIa expression, respectively (2, 11). The twins' younger sister also had asymptomatic macrothrombocytopenia. The mother was diagnosed with immune thrombocytopenia, and the father was unavailable for the study. Written informed consent was obtained from the mother in accordance with the Declaration of Helsinki. Institutional Review Boards of Nagoya Medical Center and Miyagi Children's Hospital approved this study.

Immunofluorescence analysis

Peripheral blood smears were fixed with absolute methanol, permeabilized with acetone, double-stained with anti-β1-tubulin antibody NB2301 (1 : 1000)(10) and anti-α-tubulin antibody DM1A (LabVision, Fremont, CA, USA)(1 : 200), and then reacted with Alexa 488-labeled anti-rabbit IgG and Alexa 555-labeled anti-mouse IgG (Invitrogen, Carlsbad, CA, USA). NB2301 was raised in rabbits against a synthetic peptide corresponding to C-terminal 425–451aa of human β1-tubulin. DM1A is a mouse monoclonal antibody raised against native chick brain microtubules. Chinese hamster ovary (CHO) cells transfected with *TUBB1* cDNA and mouse fetal liver-derived megakaryocytes transduced with *TUBB1* cDNA were simultaneously analyzed. Stained cells were examined under a BX50 fluorescence microscope with a 100×/1.35 numerical aperture oil objective using DP Manager software (Olympus, Tokyo, Japan).

Electron microscopy

For transmission electron microscopy, washed platelets prepared from acid-citrate-dextrose citrated whole blood were fixed in 2% glutaraldehyde and postfixed in 1% osmium tetroxide. The platelet samples were embedded in epoxy resin (Epon 812; TAAB, Berks, UK). Ultra-thin sections were cut, stained with uranyl acetate and lead citrate, and observed under a transmission electron microscope (JEM-1010, JEOL, Tokyo, Japan) (12). For negative staining, Triton X-100-extracted platelets were placed on formvar-coated carbon-stabilized grids, stained with uranyl acetate, and examined with JEM-1010 electron microscope (13).

Immunoblot analysis

Whole platelet proteins were isolated using a NucleoSpin RNA/Protein kit (Macherey-Nagel GmbH & Co., KG, Düren, Germany), separated by sodium dodecyl sulfate-polyacrylamide gel electrophoresis on 4–12% gradient acrylamide slab gels (Invitrogen), and electroblotted onto polyvinylidene difluoride membranes. The blots were incubated with anti-αIIb antibody SZ22 (Beckman-Coulter, Miami, FL, USA), DM1A, and NB2301, and reacted with horseradish peroxidase-conjugated secondary antibody. Bound antibodies were visualized using enhanced chemiluminescent substrate. Blots were densitometrically analyzed using ImageQuant software (Molecular Dynamics, Sunnyvale, CA, USA).

Mutational analysis

The entire coding sequence of exons and exon-intron boundaries of *TUBB1* was amplified by PCR, and the products were subjected to DNA sequence analysis as described (10).

Bioinformatic analysis

The multiple alignment of β1-tubulin was processed using the ClustalW program (http://www.clustal.org). The potential functional effects of the mutation was predicted using different function prediction programs, such as PROVEAN (http://www.provean.jcvi.org), Mutation Taster (http://www.mutationtaster.org), and PolyPhen2 (http://genetics.bwh.harvard.edu/pph2/). The 3D structure of β-tubulin was generated with the program MacPyMol (http://www.delanoscientific.com/) with coordinates from Protein Data Base entry 1JFF (http://www.pdb.org/).

TUBB1 transfection

TUBB1 cDNA in-frame with the C-terminal myc epitope tag cloned into pcDNA3.1 (pcDNA3.1/*TUBB1*myc)

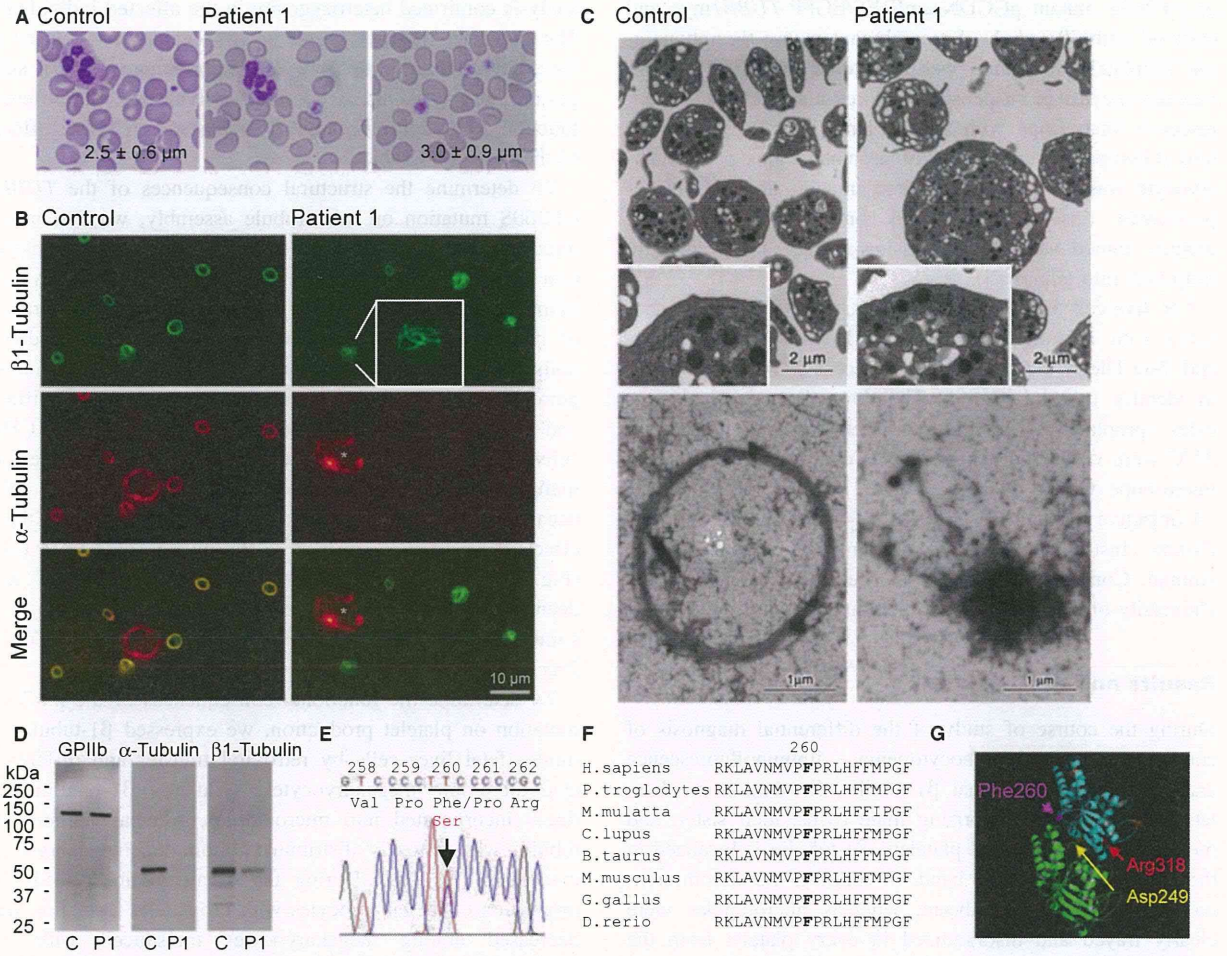

Figure 1 Platelet microtubule organization and β1-tubulin (A) Platelet morphology. Peripheral blood smears were stained with May-Grünwald Giemsa (original magnification, ×1000). The patient showed giant platelets with morphologically normal leukocytes. Numbers in each panel indicate mean platelet size (μm; $n = 200$). (B) Immunofluorescence analysis of platelet tubulin. Platelets from patient 1 lack marginal band structure, and frayed and disorganized microtubule-like structures were evident. Asterisks indicate leukocytes stained for α-tubulin. (C) Ultrastructure of platelets. Upper panels: Conventional transmission electron microscopy. Circumferential microtubules are absent in marginal region of the platelets from patient 1 (Inset). Lower panels: Negative staining. Circumferential microtubule coil was absent in the platelets from patient 1. (D) Immunoblot analysis of platelet tubulin. C, control; P1, patient 1. (E) Entire coding sequence of exons and exon-intron boundaries of *TUBB1* was amplified by PCR and subjected to direct cycle sequence analysis. A T to C transition at nucleotide 779 (c.779T > C), changing Phe260 to Ser (p.F260S), was detected. Arrow indicates position of substitution. (F) Multiple alignment of β1-tubulin. Amino acid sequence alignment of β1-tubulin is shown for human and other species. Substituted amino acid is indicated in bold. (G) Structural analysis of p.F260S using a tubulin 3D model. Arrows indicate locations of p.F260S, p.D249N, and p.R318W. Phe260 (magenta) and Asp249 (yellow) are located at, and Arg318 (red) is located near α and β intradimer interface. Blue, β-tubulin; green, α-tubulin.

(Invitrogen) was described previously (10). p.F260S mutant construct was prepared on pcDNA3.1/*TUBB1*myc by site-directed mutagenesis. CHO cells were transiently transfected with pcDNA3.1/*TUBB1*myc. At 24 h post-transfection, cells were seeded on fibronectin-coated (10 μg/mL) chamber slides (Millipore, Bedford, MA, USA) and cultured for 3 h. They were subjected to immunofluorescence analysis.

Retroviral transduction of cultured megakaryocytes

TUBB1 cDNA with the C-terminal myc epitope tag (*TUBB1*myc) was subcloned into the retroviral vector, pGCDNsamIRES/EGFP, and transfected into 293gpg packaging cells to obtain viral stocks (11, 14). Particles were pseudotyped using vesicular stomatitis virus G protein. E13.5 mouse fetal liver cells were transduced with wild type

or p.F260S mutant pGCDNsamIRES/EGFP-*TUBB1*myc and cultured with 40 ng/mL of recombinant mouse thrombopoietin. Proplatelet formation was monitored on EGFP-positive megakaryocytes in suspension cultures under an IX71 fluorescence microscope with an LCPlanFI 20×/0.40 objective lens (Olympus). The number of proplatelet tips per megakaryocyte was counted on acquired images, and the size of proplatelet tips was measured on immunofluorescence images stained with NB2301 using ImageJ 1.43u software (http://rsb.info.nih.gov/ij).

For live-cell imaging experiments, the cells were incubated with PE-conjugated anti-CD41 (MWReg30, Biolegend, San Diego, CA, USA) and Hoechst 33342 (Invitrogen) to identify megakaryocytes. The dynamics of megakaryocytes (proplatelet formation and cell rupture) cultured at 37°C were visualized using an A1R confocal laser scanning microscope with a PlanApo 100×/1.40 numerical aperture oil objective using three laser lines (405, 488, and 561 nm) (Nikon Instruments, Tokyo, Japan). The Experimental Animal Committee of Nagoya Medical Center and the University of Tokyo approved the animal studies.

Results and discussion

During the course of study of the differential diagnosis of congenital macrothrombocytopenia, immunofluorescence analysis detected abnormal β1-tubulin distribution in platelets from a family comprising male twins, their sister, and mother. In resting normal platelets, β1-tubulin is localized in the marginal microtubule band. In contrast, the circumferential ring staining was absent, whereas microtubules were clearly frayed and disorganized in every platelet from the affected individuals (Fig. 1B). Faint immunofluorescence staining indicated reduced levels of α-tubulin in platelets from patients compared with those from control patients observed under the same conditions. Under transmission microscopy, circumferential microtubules were identified lying just inside cell membrane in equatorial plane of the control platelets. In contrast, round and large platelets are evident in samples from patient 1; circumferential microtubules are absent in marginal region. Negative stain electron microscopy demonstrated organized circumferential microtubule coils, comprising about 10 microtubules in control platelets. Circumferential microtubule coil was absent in the platelets from patient 1. Microtubule coil possesses a single, straight, free end, and spreads from center of an electron-dense platelet (Fig. 1C). The expression of platelet β1-tubulin was decreased by 38%, and that of α-tubulin was decreased to 2% compared with that in control platelets (Fig. 1D). The decrease was not accompanied by a decrease of mRNA levels (data not shown).

We searched for *TUBB1* mutations and found a novel conserved p.F260S (c.779T > C) mutation located at the α- and β-tubulin intradimer interface (Fig. 1E–G)(15). Restriction analysis confirmed heterozygosity in the affected individuals. The mutation was not found in 108 healthy controls or in the SNP database (http://www.ncbi.nlm.nih.gov/SNP/), suggesting that it is not a common polymorphism. Different function prediction programmes suggested deleterious effects of the mutation (Table 2).

To determine the structural consequences of the *TUBB1* p.F260S mutation on microtubule assembly, we first monitored mutant β1-tubulin in CHO cells after transient transfection (Fig. 2A). Wild-type β1-tubulin was localized as fine filamentous cytoplasmic networks, indicating incorporation of recombinant β1-tubulin into microtubules with endogenous α-tubulin. In contrast, mutant β1-tubulin was not incorporated into microtubules, and the distribution was diffuse and partly perinuclear. Expression of β1-tubulin in CHO cells has been reported to arrest mitosis and lead to the formation of large multinucleated cells (16). The CHO cells became larger, multinucleated, and polyploid, and these effects were more prominent in the mutant-transfected cells (Fig. 2A). The expression of endogenous α-tubulin was decreased within the mutant-transfected cells, which was similar to the findings observed in platelets (Figs 1B,D and 2A).

To determine the functional consequences of the p.F260S mutation on platelet production, we expressed β1-tubulin in mouse fetal liver cells by retroviral transfer and differentiated them into megakaryocytes. Wild-type β1-tubulin was finely incorporated into microtubules, whereas mutant β1-tubulin was diffusely distributed within the megakaryocyte cytoplasm (Fig. 2B). During the 4-day culture period, the proportion of megakaryocytes with proplatelet formation was decreased among megakaryocytes transduced with the mutant. The number of proplatelet tips was decreased, and the size of the tips increased (Fig. 2C,D). Live-cell imaging showed that the extent of proplatelet formation was clearly diminished. Proplatelet elaboration was scarcely observed, and instead, large bleb protrusions were occasionally evident in mutant-transduced megakaryocytes (Fig. 2D and Video S1, S2). These findings indicated that the mutant β1-tubulin dominantly affected the microtubule assembly and impaired proplatelet formation.

Dynamic microtubule assembly and polymerization are required to regulate proplatelet formation and platelet maturation (7, 17). The coordinate levels of α- and β-tubulins are

Table 2 Functional prediction for *TUBB1* p.F260S mutation

	PROVEAN	Mutation taster	PolyPhen2
Prediction	Deleterious	Disease causing	Probably damaging
Score	−6.794	4.23	

The potential functional effects of the mutation were predicted using different function prediction programs.

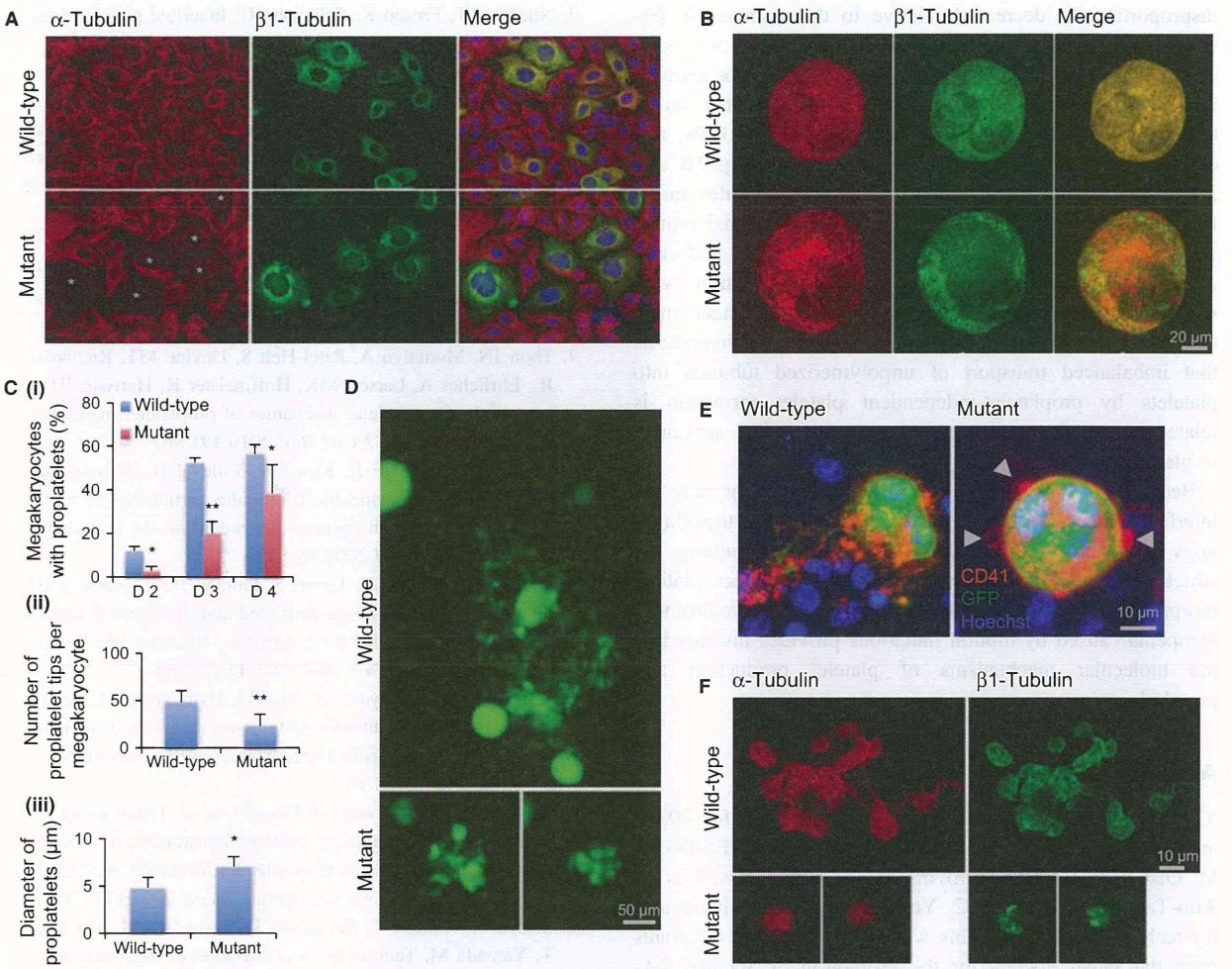

Figure 2 β1-tubulin transduction in Chinese hamster ovary (CHO) cells and mouse fetal liver-derived megakaryocytes. (A) β1-tubulin localization in CHO cells that were transiently transfected with pcDNA3.1/*TUBB1*myc. Cells were stained with antibodies to endogenous α-tubulin (red) and to the transfected β1-tubulin (green) as well as DAPI to label the DNA (blue). In merged images, CHO cells expressing wild-type β1-tubulin appear as yellow or orange, whereas cells expressing mutant β1-tubulin appear green because the expression of endogenous α-tubulin was decreased (asterisks). Cells are representative of five independent experiments. (B) Microtubule organization in β1-tubulin-transduced megakaryocytes. Cells were stained endogenous α-tubulin with DM1A (red) and the transduced β1-tubulin with anti-myc antibody (MBL, Nagoya, Japan) (green). Wild-type β1-tubulin was incorporated into microtubules, but mutant β1-tubulin was not. (C) Abnormal proplatelet formation in β1-tubulin-transduced megakaryocytes. (i) The percentage of megakaryocytes extending proplatelets was decreased in mutant-transduced cells. For each sample, 100 megakaryocytes were evaluated. (ii) The number of proplatelet tips per megakaryocyte was decreased in mutant-transduced cells. Fifty megakaryocytes per sample were evaluated. (iii) Size of proplatelet tips was increased in mutant-transduced cells. One hundred EGFP and β1-tubulin double-positive proplatelet tips per sample were evaluated. Data were analyzed using unpaired, two-tailed t-tests. $P < 0.05$ was considered statistically significant. Data are presented as mean ± SD. $*P < 0.05$, $**P < 0.001$. (D) Representative megakaryocytes extending proplatelets from three independent experiments. Fewer proplatelet tips/bulbous structures are evident, and size of tips is increased in megakaryocytes transduced with mutant. (E) Representative megakaryocytes from three independent live-cell imaging experiments. Megakaryocytes were differentiated from fetal liver cells of CAG-eGFP mice; therefore, the cytoplasm can be identified by eGFP signals (green). The cells were stained with Hoechst to identify nucleus (blue) and anti-CD41 antibody (red). Proplatelet elaboration is rare, and occasional large bleb protrusions are evident in megakaryocytes transduced with mutant (arrow heads). Original videos are available as Video S1 and S2. (F) Microtubule organization in proplatelet tips. Megakaryocyte cultures were cytospun on glass slides. Representative images from three independent experiments.

transcriptionally and translationally maintained for proper heterodimer assembly in cells, and when exogenous β-tubulin is overexpressed, the synthesis of the endogenous β-tubulin is inhibited and that of α-tubulin is upregulated (18, 19). The synthesis of β2- and β5-tubulins was increased in *TUBB1*-knockout mice (9). In contrast, α-tubulin was

disproportionally decreased relative to the decrease in β1-tubulin (Fig. 1B,D), and furthermore, β5-tubulin was substantially absent in our patients' platelets (data not shown). Defective mutant β1-tubulin would cause deregulated microtubule organization, as shown in platelets, CHO cells, and cultured megakaryocytes and proplatelet tips (Figs 1B and 2A,B,F). Thus, the deficient functional microtubules might lead to defective proplatelet formation and abnormal protrusion-like platelet release (Fig. 2D,E, Video S2). Defective microtubule organization and proplatelet formation were recently documented in Rac1- and Cdc42-deficient mice (20). Combined, these observations support the hypothesis that imbalanced transport of unpolymerized tubulins into platelets by proplatelet-independent platelet formation is related to the disorganization of microtubule-like structures in platelets.

Because p.D249N and p.R318W, locating at or near the interface, also reportedly cause macrothrombocytopenia in dogs and humans, respectively, mutations disrupting the structure of the intradimer interface might affect platelet morphology (10, 21). Analysis of congenital macrothrombocytopenia caused by tubulin mutations provides insights into the molecular mechanisms of platelet production and morphology.

Acknowledgements

The authors would like to thank R.C. Mulligan for 293gp and 293gpg cells, M. Onodera for pGCDNsamIRES/EGFP, M. Otsu for help with retroviral experiments, as well as Y. Kito-Takagi, M. Tajima, C. Yoshinaga, and T. Hirabayashi for technical assistance. This work was supported by grants from the Japan Society for the Promotion of Science KAKENHI (S.K.), Mitsubishi Pharma Research Foundation (S.K.), the 24th General Assembly of the Japanese Association of Medical Sciences (S.K.), Funding Program for Next Generation World-Leading Researchers (S.N.), and the Translational Systems Biology, Medicine Initiative (S.N.) from the Japan Science and Technology Agency.

Authorship and disclosures

S.K. designed and performed research, analyzed data, and wrote the paper; S.N. performed live-cell imaging experiments; H. Suzuki performed electron microscopic analysis; M.I. contributed patient samples; H. Saito supervised the research. The authors report no potential conflict of interests.

References

1. Balduini CL, Savoia A. Genetics of familial forms of thrombocytopenia. *Hum Genet* 2012;**131**:1821–32.
2. Kunishima S, Saito H. Congenital macrothrombocytopenias. *Blood Rev* 2006;**20**:111–21.
3. Nurden AT, Freson K, Seligsohn U. Inherited platelet disorders. *Haemophilia* 2012;**18**(Suppl 4):154–60.
4. Thon JN, Italiano JE Jr. Does size matter in platelet production? *Blood* 2012;**120**:1552–61.
5. Thon JN, Macleod H, Begonja AJ, Zhu J, Lee KC, Mogilner A, Hartwig JH, Italiano JE Jr. Microtubule and cortical forces determine platelet size during vascular platelet production. *Nat Commun* 2012;**3**:852.
6. Italiano JE Jr, Lecine P, Shivdasani RA, Hartwig JH. Blood platelets are assembled principally at the ends of proplatelet processes produced by differentiated megakaryocytes. *J Cell Biol* 1999;**147**:1299–312.
7. Thon JN, Montalvo A, Patel-Hett S, Devine MT, Richardson JL, Ehrlicher A, Larson MK, Hoffmeister K, Hartwig JH, Italiano JE Jr. Cytoskeletal mechanics of proplatelet maturation and platelet release. *J Cell Biol* 2010;**191**:861–74.
8. Lecine P, Italiano JE Jr, Kim SW, Villeval JL, Shivdasani RA. Hematopoietic-specific β1 tubulin participates in a pathway of platelet biogenesis dependent on the transcription factor NF-E2. *Blood* 2000;**96**:1366–73.
9. Schwer HD, Lecine P, Tiwari S, Italiano JE Jr, Hartwig JH, Shivdasani RA. A lineage-restricted and divergent β-tubulin isoform is essential for the biogenesis, structure and function of blood platelets. *Curr Biol* 2001;**11**:579–86.
10. Kunishima S, Kobayashi R, Itoh TJ, Hamaguchi M, Saito H. Mutation of the β1-tubulin gene associated with congenital macrothrombocytopenia affecting microtubule assembly. *Blood* 2009;**113**:458–61.
11. Kunishima S, Kashiwagi H, Otsu M, *et al.* Heterozygous ITGA2B R995W mutation inducing constitutive activation of the αIIbβ3 receptor affects proplatelet formation and causes congenital macrothrombocytopenia. *Blood* 2011;**117**:5479–84.
12. Suzuki H, Kaneko T, Sakamoto T, Nakagawa M, Miyamoto T, Yamada M, Tanoue K. Redistribution of α-granule membrane glycoprotein IIb/IIIa (integrin αIIbβ3) to the surface membrane of human platelets during the release reaction. *J Electron Microscopy* 1994;**43**:282–9.
13. White JG, Krumwiede M. Isolation of microtubule coils from normal human platelets. *Blood* 1985;**65**:1028–32.
14. Kunishima S, Okuno Y, Yoshida K, *et al.* ACTN1 mutations cause congenital macrothrombocytopenia. *Am J Hum Genet* 2013;**92**:431–8.
15. Lowe J, Li H, Downing KH, Nogales E. Refined structure of αβ-tubulin at 3.5 a resolution. *J Mol Biol* 2001;**313**:1045–57.
16. Yang H, Ganguly A, Yin S, Cabral F. Megakaryocyte lineage-specific class VI β-tubulin suppresses microtubule dynamics, fragments microtubules, and blocks cell division. *Cytoskeleton* 2011;**68**:175–87.
17. Patel-Hett S, Richardson JL, Schulze H, *et al.* Visualization of microtubule growth in living platelets reveals a dynamic marginal band with multiple microtubules. *Blood* 2008;**111**:4605–16.
18. Cleveland DW. Autoregulated instability of tubulin mRNAs: a novel eukaryotic regulatory mechanism. *Trends Biochem Sci* 1988;**13**:339–43.

19. Gonzalez-Garay ML, Cabral F. Overexpression of an epitope-tagged β-tubulin in Chinese hamster ovary cells causes an increase in endogenous alpha-tubulin synthesis. *Cell Motil Cytoskeleton* 1995;**31**:259–72.
20. Pleines I, Dutting S, Cherpokova D, *et al.* Defective tubulin organization and proplatelet formation in murine megakaryocytes lacking Rac1 and Cdc42. *Blood* 2013;**122**:3178–87.
21. Davis B, Toivio-Kinnucan M, Schuller S, Boudreaux MK. Mutation in β1-tubulin correlates with macrothrombocytopenia in Cavalier King Charles Spaniels. *J Vet Intern Med* 2008;**22**:540–5.

Supporting Information

Additional Supporting Information may be found in the online version of this article:

Video S1. Live-cell imaging of platelet release. Original movie of Figure 2E (left, wild type).

Video S2. Live-cell imaging of platelet release. Original movie of Figure 2E (right, mutant).

Sakata et al. Thrombosis Journal 2014, 12:1
http://www.thrombosisjournal.com/content/12/1/1

THROMBOSIS JOURNAL

ORIGINAL BASIC RESEARCH Open Access

Paxillin is an intrinsic negative regulator of platelet activation in mice

Asuka Sakata[1,2], Tsukasa Ohmori[1*], Satoshi Nishimura[1,3,4], Hidenori Suzuki[5], Seiji Madoiwa[1], Jun Mimuro[1], Kazuomi Kario[2] and Yoichi Sakata[1]

Abstract

Background: Paxillin is a LIM domain protein localized at integrin-mediated focal adhesions. Although paxillin is thought to modulate the functions of integrins, little is known about the contribution of paxillin to signaling pathways in platelets. Here, we studied the role of paxillin in platelet activation in vitro and in vivo.

Methods and results: We generated paxillin knockdown (Pxn-KD) platelets in mice by transplanting bone marrow cells transduced with a lentiviral vector carrying a short hairpin RNA sequence, and confirmed that paxillin expression was significantly reduced in platelets derived from the transduced cells. Pxn-KD platelets showed a slight increased in size and augmented integrin αIIbβ3 activation following stimulation of multiple receptors including glycoprotein VI and G protein-coupled receptors. Thromboxane A_2 biosynthesis and the release of α-granules and dense granules in response to agonist stimulation were also enhanced in Pxn-KD platelets. However, Pxn-KD did not increase tyrosine phosphorylation or intracellular calcium mobilization. Intravital imaging confirmed that Pxn-KD enhanced thrombus formation in vivo.

Conclusions: Our findings suggest that paxillin negatively regulates several common platelet signaling pathways, resulting in the activation of integrin αIIbβ3 and release reactions.

Keywords: Platelet, Glycoprotein, Platelet aggregation, Release reaction

Background

A breakdown of normal platelet function results in either unexpected bleeding or thrombotic events [1]. Platelets are inactive in the intact vasculature under physiological conditions. However, once the platelets encounter an injured region of the endothelium, they attach through an interaction between von Willebrand factor and the glycoprotein (GP) Ib/IX/V complex [2], and then collagen receptor GPVI triggers platelet activation. Activated platelets release several classes of agonists, including ADP and thromboxane (Tx) A_2, which promote further platelet activation [3]. These steps ultimately increase the affinity of integrin αIIbβ3 for its ligands and induce platelet aggregation [4]. The intracellular signaling that increases the affinity of integrins is known as inside-out signaling [4]. Multiple signal transduction pathways from various receptors share common inside-out signaling cascades. For example, phosphoinositol hydrolysis, which leads to calcium mobilization and protein kinase C activation [5], and Rap1b activation are well-known signaling pathways that regulate integrin-mediated platelet functions [6].

To increase the affinity of integrin αIIbβ3, inside-out signaling pathways induce a drastic conformational change of the integrin [7]. Direct interactions between cytoskeletal proteins (e.g., talin and kindlin) and cytoplasmic β integrin are essential for inducing the conformational change of integrins [7]. Indeed, the loss of talin or kindlin in platelets dramatically reduces integrin αIIbβ3-mediated platelet aggregation, despite normal expression levels of the surface receptors [8,9]. Selective blockade of talin binding by a single amino acid substitution in β3 integrin also impairs integrin αIIbβ3-dependent platelet responses [10]. Although a number of integrin-associated proteins have been reported [11], the identities of proteins and their roles in regulating integrin signaling in platelets have not been fully characterized. It is also unknown whether

* Correspondence: tohmori@jichi.ac.jp
[1]Research Division of Cell and Molecular Medicine, Center for Molecular Medicine, Jichi Medical University School of Medicine, 3111-1 Yakushiji, Shimotsuke, Tochigi 329-0498, Japan
Full list of author information is available at the end of the article

additional molecules, other than talin and kindlin, are capable of regulating integrin signaling pathways.

Paxillin is a LIM domain protein that was originally identified as a substrate for oncogene *v-src* [12]. Paxillin contains two conserved structural domains, the N-terminus and C-terminus, which consist of four LIM domains [13,14]. Two other family members have also been identified, Hic-5 and leupaxin [13,14]. Paxillin is ubiquitously expressed alongside these variants [13,14], except in human platelets that predominantly express Hic-5 [15,16]. Conversely, mouse platelets express paxillin and leupaxin in addition to Hic-5 [17]. Considering the multiple interaction motifs located within its structure, paxillin appears to serve as a signaling platform for the recruitment of numerous regulatory proteins near integrins [13,14]. Paxillin directly interacts with the cytoplasmic domain of integrin α4 and α9, but not αIIb, and these interactions controls integrin-mediated cell migration and spreading [18,19].

Integrin αIIbβ3 in platelets is suitable for studies of integrin receptors because its ligand binding and signal transduction pathways are well characterized. Elucidating the intracellular proteins involved in the activation of integrin αIIbβ3 can provide a better understanding of the functions of integrins and might result in the discovery of new antithrombotic targets [20]. We previously reported that lentiviral vector-mediated short hairpin RNA (shRNA) expression in hematopoietic stem cells greatly reduces the expression of the target protein in platelets [21]. This method enables functional analyses of target proteins that modulate platelet activation in anucleate platelets [21]. In the present study, we used this method to investigate the roles of paxillin in platelet activation, and found that paxillin negatively regulates platelet signaling pathways including the activation of integrin αIIbβ3 and release reactions.

Materials and methods

Materials

All mouse cytokines were purchased from PeproTech (London, UK). The following antibodies and agonists were obtained from the specified suppliers: PAC-1 monoclonal antibody (mAb), anti-mouse P-selectin mAb (RB40.34), anti-paxillin mAb (clone 349), and anti-Hic-5 mAb (BD Biosciences, San Jose, CA); horseradish peroxidase-conjugated anti-green fluorescent protein (GFP) polyclonal antibody (Acris Antibodies, Himmelreich, Germany); phycoerythrin (PE)-Cy7-conjugated anti-mouse IgM (eBioscience, San Diego, CA); anti-talin mAb (clone 8D4); anti-phosphotyrosine mAb (clone 4G10), and BAPTA-AM (Millipore, Billerica MA); human fibrinogen and epinephrine (Sigma-Aldrich, St. Louis, MO); anti-vinculin mAb (V284) (Chemicon, Billerica, MA); anti-mouse GPVI mAb (Six.E10), anti-mouse GPIbα mAb (Xia.G5), and anti-mouse integrin αIIbβ3 mAb (Leo.D2 and clone JON/A) (Emfret Analytics, Eibelstadt, Germany); anti-α-actin mAb (D6F6), anti-FAK polyclonal antibody, and anti-Src mAb (32G6) (Cell Signaling Technology, Danvers, MA); anti-Rap1b polyclonal antibody and anti-protein kinase Cα mAb (M4) (Upstate Cell Signaling Solutions, Lake Placid, NY); allophycocyanin (APC)-conjugated anti-rat IgG polyclonal antibody (R& D Systems, Minneapolis, MN); convulxin (ALEXIS Biochemicals, Plymouth Meeting, PA); AYPGKF (Invitrogen, Carlsbad, CA); ADP (MC medical, Tokyo, Japan); U46619 (Cayman Chemical, Ann Arbor, MI).

Lentiviral vector and virus production

A lentiviral vector plasmid for expression of shRNA sequences and GFP (LentiLox vector) was purchased from the American Type Culture Collection (Manassas, VA) [22]. To efficiently express GFP in platelets, the cytomegalovirus promoter of the LentiLox vectors was substituted with the platelet-specific GPIbα promoter (LentiLox-GPIbα) [21]. Putative shRNA sequences were designed using web-based software provided by Thermo Scientific Molecular Biology (http://www.thermoscientificbio.com/design-center/). Three shRNA sequences were synthesized for mouse paxillin and then cloned into a LentiLox vector plasmid (Additional files 1 and 2). Lentiviruses were produced as described previously [23].

Transplantation of mouse bone marrow cells

All animal procedures were approved by the Institutional Animal Care and Concern Committee of Jichi Medical University, and animal care was performed in accordance with the committee's guidelines. Mouse bone marrow cells (C57BL/6 J) were isolated and resuspended in StemPro®-34 SFM medium (Invitrogen) supplemented with 100 ng/mL each of stem cell factor, thrombopoietin, interleukin-6, and fms-like tyrosine kinase 3 ligand, and 200 ng/mL soluble interleukin-6 receptor. The lentiviral vector was added at 12–16 h after cell isolation (multiplicity of infection [MOI] = 5), and the cell culture was continued for 21–22 h. Each recipient mouse (8–12 weeks of age) was irradiated with a single lethal dose of 9.5 Gy and then intravenously injected with 2×10^6 lentivirus-transduced bone marrow cells. After transplantation, about 50% of platelets expressed GFP (Figure 1). Mice with 70% of their platelets exhibiting GFP positivity were used in experiments that could not distinguish GFP-positive platelets, *i.e.*, light transmission aggregometry, clot retraction, release concentration, calcium mobilization, and intravital microscopy.

Immunoblotting

Immunoblotting with the specific antibodies was performed as described previously [21]. To assess protein tyrosine phosphorylation, washed platelets were pretreated

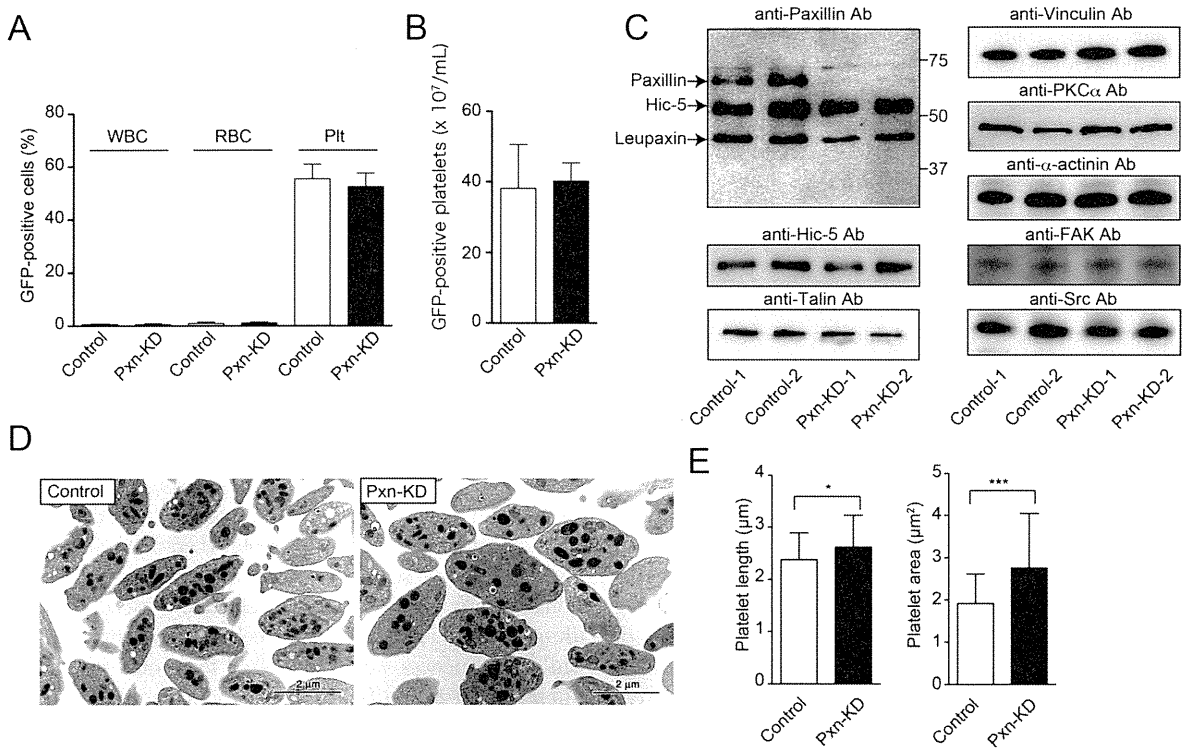

Figure 1 Characterization of Pxn-KD platelets. Bone marrow cells transduced with LentiLox-sh-control-GPIbα (Control) or LentiLox-sh-paxillin-GPIbα (Pxn-KD) at an MOI of 5 were transplanted into lethally irradiated recipient mice. **(A)** The numbers of GFP-positive cells (%) among white blood cells (WBCs), red blood cells (RBCs), and platelets (Plts) in peripheral blood at 30 days after transplantation were assessed by flow cytometry. Columns and error bars represent the mean ± s.d. ($n = 10$). **(B)** Absolute number of GFP-positive platelets in peripheral blood at 30 days after transplantation. Columns and error bars represent the mean ± s.d. ($n = 10$). **(C)** Platelet lysates were immunoblotted with the indicated antibodies. Data are for two mice with >80% of platelets expressing GFP in each experiment. **(D)** The morphology of control and Pxn-KD platelets was examined by transmission electron microscopy. Bars = 2 μm. **(E)** Platelet length (left panel) and area (right panel) were quantified by ImageJ software. Columns and error bars represent the mean ± s.d. ($n = 53–72$). Statistical significance was determined by the Student's *t*-test. $^*P < 0.05$ and $^{***}P < 0.001$ vs. control.

with 1 mmol/L EDTA, 5 U/mL apyrase, and 10 μmol/L SQ29548 to exclude the effects of aggregation, released ADP, and TxA_2.

Transmission electron microscopy

Mouse platelet pellets were fixed in 2% glutaraldehyde in 0.1 mol/L phosphate buffer (pH 7.4) for 60 min at 4°C. The samples were washed, post-fixed with 1% osmium tetroxide in 0.1 mol/L phosphate buffer for 60 min at 4°C, dehydrated with a graded ethanol series, and then embedded in Epon (TAAB Laboratories, Aldermaston, UK) as described previously [24]. Ultrathin sections were prepared, stained with uranyl acetate and lead citrate, and then examined under a JEM1010 transmission electron microscope (JEOL, Tokyo, Japan) at an accelerating voltage of 80 kV. The length and area of platelets were quantified using ImageJ Ver. 10.2 for Macintosh (NIH, Bethesda, MD).

Preparation of washed mouse platelets and flow cytometry

A blood sample (100–400 μL) was drawn from each mouse through the right jugular vein using a 30 G syringe containing 1/10 sodium citrate, and then diluted with 3 mL Hepes/Tyrode buffer (138 mmol/L NaCl, 3.3 mmol/L NaH_2PO_4, 2.9 mmol/L KCl, 1 mmol/L $MgCl_2$, 1 mg/mL glucose, and 20 mmol/L Hepes, pH 7.4). The diluted blood was centrifuged at $120 \times g$ for 8 min, and the platelets obtained from the platelet-rich fraction were washed and resuspended in Hepes/Tyrode buffer. Just prior to centrifugation, a 15% acid-citrate-dextrose A solution and 0.1 μmol/L prostaglandin I_2 were added to inhibit platelet activation. The final platelet suspensions were adjusted to 1×10^7 platelets/mL and supplemented with 1 mmol/L $CaCl_2$. To assess the binding of JON/A, a monoclonal antibody (mAb) that recognizes activated mouse αIIbβ3 [25], to platelets, 30 μL of washed platelets was incubated with 4 μL of agonist solution, 4 μL of phycoerythrin (PE)-

conjugated JON/A and 1 μL of biotin-conjugated anti-mouse P-selectin mAb for 5 min, and then supplemented with 1 μL of allophycocyanin (APC)-conjugated streptavidin. After 15 min of incubation, JON/A binding and P-selectin expression were determined by flow cytometry using a FACSAria Cell Sorter (Becton Dickinson, Mountain View, CA). Antibody binding was quantified as the mean fluorescence intensity (MFI) of GFP-positive platelets.

Platelet aggregation

Washed platelets were prepared as described above. The final suspensions were adjusted to 2×10^8 platelets/mL and supplemented with 1 mmol/L $CaCl_2$ and 200 μg/mL fibrinogen. The aggregation response to agonist stimulation was measured based on light transmission measured using a PA-200 platelet aggregation analyzer (Kowa, Tokyo, Japan).

Measurement of platelet products

Washed platelets (2×10^8/mL) were stimulated with the indicated agonists for 15 min, and then the supernatants were recovered by centrifugation. The levels of platelet factor 4 (PF4) and serotonin in the supernatants were measured using a mouse PF4 enzyme-linked immunosorbent assay (ELISA) kit (R & D Systems) and an anti-serotonin ELISA kit (GenWay Biotech, San Diego, CA), respectively. The levels of TxB_2 in the supernatants were measured using an enzyme immunoassay (Cayman Chemical).

Platelet adhesion

Platelet adhesion to fibrinogen was assessed as described previously [21]. Briefly, eight-well dishes (Lab-Tek® Chamber Slide™) were coated with 400 μg/mL fibrinogen and then blocked with 1 mg/mL bovine serum albumin (BSA). Platelets were then added to the fibrinogen-coated dishes and incubated for 30 min at 37°C. Adherent platelets were fixed with 3% paraformaldehyde and then permeabilized with phosphate-buffered saline (PBS) containing 0.3% Triton X-100 and 5% donkey serum. After washing with PBS, the platelets were incubated with an anti-GFP polyclonal antibody (MBL, Aichi, Japan). Bound antibodies were detected by Alexa Fluor 488-conjugated anti-rabbit IgG. Actin filaments were detected by staining with 1 μg/mL rhodamine-conjugated phalloidin. Immunofluorescence staining was observed and photographed under a confocal microscope (FV1000; Olympus, Tokyo, Japan). The spread area of GFP-positive platelets was quantified using ImageJ software. Because Pxn-KD platelets were slightly larger than control platelets (Figure 1), the mean platelet size determined by BSA staining was subtracted from the total area on fibrinogen to calculate the actual increase in platelet spreading.

Clot retraction

Human platelet-poor plasma was mixed with the same volume of Hepes/Tyrode buffer containing washed mouse platelets (final concentration: 3×10^8 platelets/ml). Plasma coagulation was initiated by addition of 0.1 U/mL thrombin. The clots were photographed at various time points after thrombin addition. When indicated, 0.5 mmol/L manganese was added to exclude the role of inside-out signaling. The two-dimensional area of serum formation extruded by clot retraction was quantified using ImageJ software and expressed as the progression of clot retraction.

Calcium mobilization

Platelets were incubated with GFP-Certified™ FluoForte™ dye (Enzo Life Sciences, Farmingdale, NY). The fluorophore-loaded platelets (2×10^8/mL) were resuspended in Hepes-Tyrode buffer containing 1 mmol/L EDTA, 5 U/mL apyrase, and 10 μmol/L SQ29548 to exclude the effects of aggregation, extracellular calcium, released ADP, and TxA_2. After stimulation, the intracellular calcium concentration was determined by monitoring the fluorescence (excitation, 530 nm; emission, 570 nm) using a microplate spectrofluorometer (Gemini EM; Molecular Devices, Sunnyvale, CA).

Intravital microscopy and thrombus formation

Intravital microscopy was performed to analyze thrombus formation in vivo as reported previously [26]. Briefly, Texas Red-dextran (100 mg/kg body weight [BW], molecular weight: 70 kDa; Invitrogen), Hoechst 33342 (10 mg/kg BW; Invitrogen), Dylight 488-conjugated anti-CD42b antibody (200 μg/kg BW; Emfret), and hematoporphyrin (5 mg/kg BW; Sigma) were injected into anesthetized mice to produce reactive oxygen species (ROS) following laser irradiation. Blood cell dynamics were visualized during laser excitation (wavelengths 405, 488, and 561 nm; 1.5 mW total power at 100× objective lens). After laser irradiation, sequential images of the mesentery were obtained using a resonance scanning confocal microscope (Nikon A1R; Nikon, Tokyo, Japan). The areas of thrombus (shown by anti-CD42b antibody signals) before and after laser irradiation were calculated using NIS-Elements AR 3.2 (Nikon). When indicated, thrombus formation in the femoral artery was triggered by topical application of a filter paper tip saturated with 10% $FeCl_3$. After injection of Texas Red-dextran, Hoechst 33342, and Dylight 488-conjugated anti-CD42b antibody, thrombus formation was visualized and monitored by confocal microscopy using two photon microscopy (excitation wavelength 840 nm) by NikonA1R MP (Nikon).

Bleeding time

The distal tail tip (5 mm) of an anesthetized mouse was clipped, and the tail was immediately immersed in PBS

at 37°C. Tail bleeding times were defined as the time required for the bleeding to stop.

Results

Generation of paxillin knockdown (Pxn-KD) platelets

To address the function of paxillin in mouse platelets, we used a lentiviral vector carrying shRNA sequences and GFP [22]. We synthesized three shRNA sequences for mouse paxillin, and cloned them into a LentiLox vector plasmid (Additional files 1 and 2). We selected one sequence that significantly inhibited paxillin expression in embryonic fibroblasts after transduction (Pxn-1 sequence; Additional files 1 and 2). After transplantation of bone marrow cells transduced with either the control or Pxn-KD sequence, about 50% of the platelets expressed GFP, and the absolute numbers of GFP-positive platelets did not differ between experiments using control and Pxn-KD sequences (Figure 1A–B). Furthermore, there was no effect on the total number of platelets (control: $6.8 \pm 1.72 \times 10^8$/mL; Pxn-KD: $7.7 \pm 0.65 \times 10^8$/mL, $P = 0.18$). We compared the platelet aggregation response and release reaction in platelets from wild-type C57BL/6 J and control mice, and confirmed that platelet aggregation as well as the release reaction did not differ (data not shown). To confirm knockdown of paxillin in GFP-positive platelets, we selected mice in which more than 80% of platelets expressed GFP after transplantation. Immunoblotting of platelet lysates with an anti-paxillin mAb (clone 349) showed a marked reduction in paxillin expression following transplantation of bone marrow cells transduced with the Pxn-KD sequence (Figure 1C). This antibody also recognizes other members of the paxillin family, including Hic-5 and leupaxin [17]. However, Hic-5 and leupaxilin were not affected by expression of the Pxn-KD sequence (Figure 1C). Transmission electron microscopy of resting platelets revealed that the Pxn-KD platelets were slightly larger than control platelets (Figure 1D–E). This change was largely dependent on an increase of the cytoplasm volume, but not the granule volume (Additional file 3). Pxn-KD platelets showed marginally elevated expression levels of GPIb and integrin αIIbβ3, even though GPVI expression was normal (Additional file 4). These changes in Pxn-KD platelets were supposed to result from the increase in platelet size.

Augmentation of integrin αIIbβ3 activation in Pxn-KD platelets

We first focused on the role of paxillin in integrin αIIbβ3 activation that is critical for platelet aggregation. We performed flow cytometric analysis of integrin αIIbβ3 activation using an anti-JON/A mAb [25]. GFP-positive Pxn-KD platelets (Figure 2A, lower panel) showed significantly enhanced αIIbβ3 activation following stimulation compared with that of control platelets (Figure 2A, upper panel). Enhanced JON/A binding of Pxn-KD platelets was observed following stimulation with the GPVI agonist convulxin and G protein-coupled receptor agonists including a protease-activated receptor 4 agonist (AYPGKF), ADP, and U46619 (Figure 2A–B). However, JON/A binding was not enhanced in unstimulated or epinephrine-stimulated platelets, suggesting that Pxn-KD alone does not induce activation of integrin αIIbβ3. We next used light transmission aggregometry to assess platelet aggregation in vitro. We found that platelet aggregation was significantly augmented in Pxn-KD platelets, and this effect was evident at low agonist concentrations that induce platelet aggregation (Figure 2C–D).

Enhanced release reactions and Tx biosynthesis in Pxn-KD platelets

We next assessed the release reactions in response to stimulation. To address the role of paxillin in α-granule secretion, P-selectin expression was determined in GFP-positive platelets by flow cytometry. As shown in Figure 3A–B, P-selectin expression in Pxn-KD platelets was significantly increased following stimulation with convulxin, AYPGKF, and U46619. In contrast, P-selectin expression was not increased by stimulation with ADP or epinephrine. We observed negligible increases in P-selectin expression of Pxn-KD platelets under the resting condition and after incubation with the fibronectin peptide Gly-Arg-Gly-Asp-Ser (GRGDS) (Figure 3B). To examine whether Pxn-KD platelets are already activated during circulation, we compared P-selectin expression in washed platelets and whole blood platelets before the preparation. An increase of P-selectin expression after washing the platelet preparation was observed in Pxn-KD platelets (30.0 ± 9.71 to 37.2 ± 5.72 in the control vs. 27.8 ± 2.56 to 44.8 ± 7.87, $P < 0.05$), suggesting that the susceptibility of Pxn-KD platelets caused marginal activation during washing. Although PF4 and serotonin content in resting platelets did not differ between control and Pxn-KD platelets (Additional file 3), the actual release of PF4 and serotonin into the supernatant in response to platelet activation was also enhanced in Pxn-KD platelets (Figure 3C–D). Of note, a marked increase in TxB_2 biosynthesis was observed in Pxn-KD platelets (Figure 3E). Pretreatment with the ADP scavenger apyrase and thromboxane A_2 receptor antagonist SQ29548 somewhat corrected the increase of JON/A binding in Pxn-KD platelets. This result suggests that the extent of the increase of integrin activation is partially dependent on the release reaction (Additional file 5). Collectively, these data suggest that paxillin negatively regulates platelet activation signaling pathways leading to integrin activation, release reactions, and Tx synthesis. It is possible that general pathway (s) involved in platelet activation were enhanced by Pxn-KD, because platelet activation was increased in

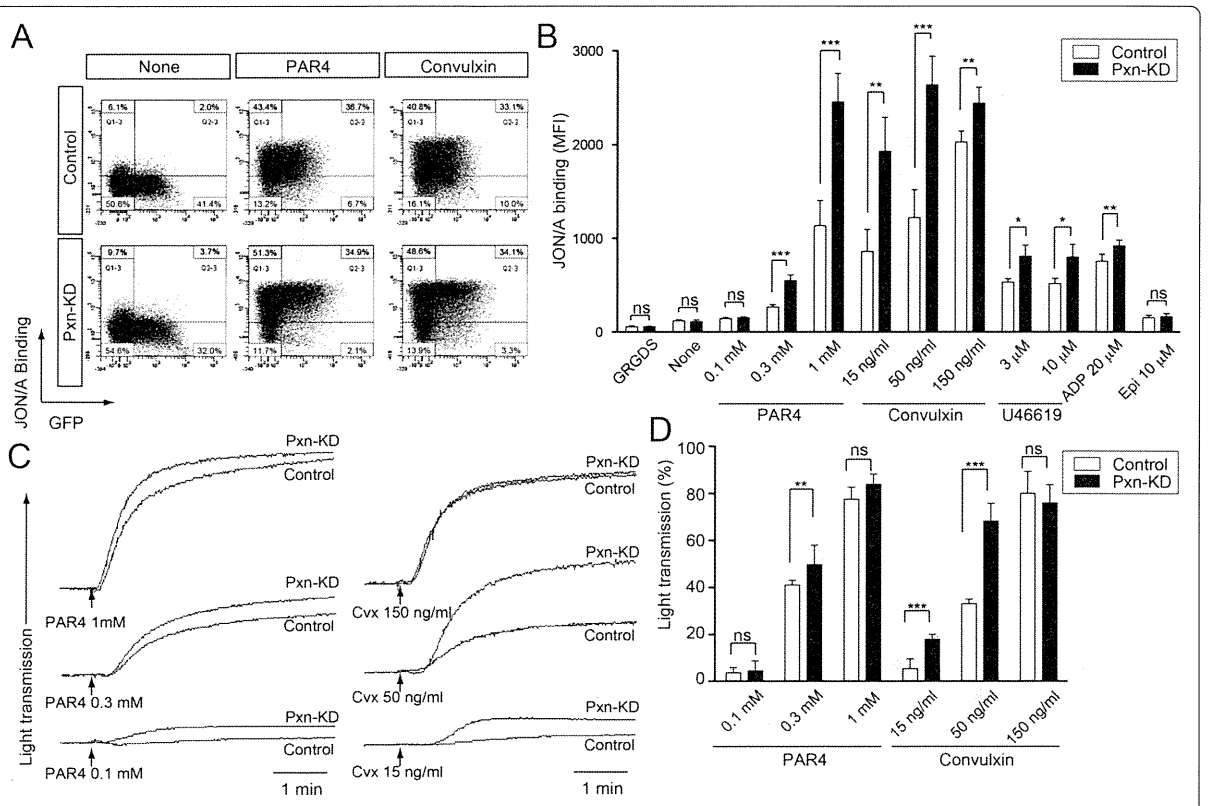

Figure 2 Pxn-KD in platelets increases agonist-induced integrin αIIbβ3 activation. Bone marrow cells transduced with LentiLox-sh-control-GPIbα (Control) or LentiLox-sh-paxillin-GPIbα (Pxn-KD) at an MOI of 5 were transplanted into lethally irradiated recipient mice. **(A)** Activation of integrin αIIbβ3 was assessed by JON/A binding to platelets incubated with or without 1 mmol/L AYPGKF or 50 ng/mL convulxin. The plots represent the degree of GFP expression (horizontal) and binding of JON/A, a monoclonal antibody that recognizes activated integrin αIIbβ3 (vertical). **(B)** Columns and error bars represent the mean ± s.d. of the MFI of JON/A binding after stimulating GFP-positive platelets with the indicated agonists ($n = 3–5$). **(C)** Platelet aggregation induced by the indicated concentration of AYPGKF or convulxin was monitored by light transmission aggregometry. **(D)** Columns and error bars represent the mean ± s.d. of maximal platelet aggregation after stimulation ($n = 5$). Open bars: control platelets; black bars: Pxn-KD platelets. Statistical significance was determined by the Student's *t*-test. $^*P < 0.05$, $^{**}P < 0.01$, and $^{***}P < 0.001$.

response to several classes of activators including GPVI and G protein-coupled receptors.

Assessment of outside-in signaling pathways in Pxn-KD platelets

To address the role of paxillin in outside-in signaling of integrin αIIbβ3, we assessed platelet spreading on fibrinogen and clot retraction. The cell area independent of integrin outside-in signaling (i.e., adherent to the BSA control) was slightly increased in Pxn-KD platelets compared with that in control platelets (data not shown), because the Pxn-KD platelets were marginally larger than control platelets (Figure 1). To quantify the increase in platelet spreading, the mean platelet size on BSA was subtracted from the total spreading area on fibrinogen. As shown in Figure 4A, the increase in platelet spreading on fibrinogen without or with convulxin stimulation was significantly greater for Pxn-KD platelets than that for control platelets (Figure 4A–B). In addition, clot retraction induced by thrombin was significantly enhanced in Pxn-KD platelets compared with that in control platelets (Figure 4C–D). Acceleration of clot retraction in Pxn-KD platelets was also observed in the presence of manganese at 15 min (6.98 ± 0.130 vs. 7.56 ± 0.072, $P < 0.05$). These observations suggest that paxillin is an important regulator of integrin outside-in signaling via integrin αIIbβ3.

The role of paxillin in calcium mobilization in platelets

Because GPVI initiates signaling cascades by activation of non-receptor tyrosine kinases, we assessed tyrosine phosphorylation elicited by the GPVI signaling pathway. As a result, tyrosine phosphorylation events induced by convulxin were not affected by Pxn-KD (Figure 5A). The agonist-induced increase in intracellular calcium mobilization is an important common and proximal signaling event controlling platelet activation. Therefore, we next examined whether Pxn-KD enhanced intracellular calcium mobilization following stimulation. To exclude